

# **Population heterogeneity in the epithelial to mesenchymal transition is controlled by NFAT and phosphorylated Sp1**

Russell Gould<sup>‡</sup> and David M. Bassen, Anirikh Chakrabarti, Jeffrey D. Varner and Jonathan Butcher<sup>‡\*</sup>

Robert Frederick Smith School of Chemical and Biomolecular Engineering and <sup>‡</sup>Nancy E. and Peter C. Meinig School of Biomedical Engineering, Cornell University, Ithaca NY 14853

**Running Title:** Modeling of TGF- $\beta$  induced EMT

**Character count:** 56,659

\*Corresponding author:

Jonathan T. Butcher,

Associate Professor, Nancy E. and Peter C. Meinig School of Biomedical Engineering,  
304 Weill Hall, Cornell University, Ithaca NY, 14853

Email: jtb47@cornell.edu

Phone: (607) 255 - 3575

Fax: (607) 255 - 7330

## Abstract

Epithelial to mesenchymal transition (EMT) is an essential differentiation program during tissue morphogenesis and remodeling. EMT is induced by soluble transforming growth factor  $\beta$  (TGF- $\beta$ ) family members, and restricted by vascular endothelial growth factor family members. While many downstream molecular regulators of EMT have been identified, these have been largely evaluated individually without considering potential crosstalk. In this study, we created an ensemble of dynamic mathematical models describing TGF- $\beta$  induced EMT to better understand the operational hierarchy of this complex molecular program. These models incorporate mass action kinetics within an ordinary differential equation (ODE) framework to describe the transcriptional and post-translational regulatory events driving EMT. Model parameters were estimated from multiple data sets using multiobjective optimization, in combination with cross-validation. TGF- $\beta$  exposure drove the model population toward a mesenchymal phenotype, while an epithelial phenotype was maintained following vascular endothelial growth factor A (VEGF-A) exposure. Simulations predicted that the transcription factors phosphorylated SP1 and NFAT were master regulators promoting or inhibiting EMT, respectively. Surprisingly, simulations also predicted that a cellular population could exhibit phenotypic heterogeneity (characterized by a significant fraction of the population with both high epithelial and mesenchymal marker expression) if treated simultaneously with TGF- $\beta$  and VEGF-A. We tested this prediction experimentally in both MCF10A and DLD1 cells and found that upwards of 45% of the cellular population acquired this hybrid state in the presence of both TGF- $\beta$  and VEGF-A. We experimentally validated the predicted NFAT/Sp1 signaling axis for each phenotype response. Lastly, we found that cells in the hybrid state had significantly different functional behavior when compared to VEGF-A or TGF- $\beta$  treatment alone. Together, these results establish a predictive mechanistic model of EMT susceptibility, and potentially reveal a novel signaling axis which regulates carcinoma progression through an EMT versus tubulogenesis response.

## **Author Summary**

Tissue formation and remodeling requires a complex and dynamic balance of interactions between epithelial cells, which reside on the surface, and mesenchymal cells that reside in the tissue interior. During embryonic development, wound healing, and cancer, epithelial cells transform into a mesenchymal cell to form new types of tissues. It is important to understand this process so that it can be controlled to generate beneficial effects and limit pathological differentiation. Much research over the past 20 years has identified many different molecular species that are relevant, but these have mainly been studied one at a time. In this study, we developed and implemented a novel computational strategy to interrogate all of the known players in this transformation process to identify which are the major bottlenecks. We determined that NFATc1 and pSP1 are essential for promoting epithelial or mesenchymal differentiation, respectively. We then predicted the existence of a partially transformed cell that exhibits both epithelial and mesenchymal characteristics. We found this partial cell type develops a network of invasive but stunted vascular structures that may be a unique cell target for understanding cancer progression and angiogenesis.

## **1 Introduction**

- 2 The epithelial to mesenchymal transition (EMT) is a broadly participating, evolutionarily  
3 conserved differentiation program essential for tissue morphogenesis, remodeling and  
4 pathological processes such as cancer (Thiery, 2003). During EMT polarized, tightly ad-  
5 hered epithelial cell monolayers are transformed into non-interacting motile mesenchymal  
6 cells that simultaneously degrade and synthesize extracellular matrix (ECM) components  
7 and invade into the underlying tissue space (Stahl & Felsen, 2001). EMT is the funda-  
8 mental initiator of developmental processes such as embryonic gastrulation and valvulo-  
9 genesis (Eisenberg & Markwald, 1995) (also Kalluri J Clin Invest 2009, Thiery Cell 2009).  
10 Transforming growth factor  $\beta$  (TGF- $\beta$ ) family members are important inducers of both de-

11 developmental and pathological EMT (Xu *et al.*, 2009, Zavadil & Böttinger, 2005). Decades  
12 of research has focused on identifying molecular regulators of EMT, but almost all on a  
13 single gene and in a nearly binary yes/no level of qualitative understanding. Medici and  
14 coworkers recently identified a core signaling program by which TGF- $\beta$  isoforms induce  
15 EMT across a variety of cell lines (Medici *et al.*, 2006, 2008). This program involves  
16 carefully orchestrated rounds of gene expression driven by the Smad and Snail families  
17 of transcription factors as well as other key factors such as lymphoid enhancer-binding  
18 factor 1 (LEF-1), nuclear factor of activated T-cells, cytoplasmic 1 (NFATc1), and speci-  
19 fity protein 1 (Sp1). Coregulators such as  $\beta$ -catenin, NF- $\kappa$ B, and the ErbB family of  
20 receptor tyrosine kinases however also participate in EMT regulation, but the degree of  
21 each's influence is difficult to ascertain in isolation (Hardy *et al.*, 2010, Huber *et al.*, 2004,  
22 Jiang *et al.*, 2007, Kim *et al.*, 2002). EMT also exhibits complex temporal dynamics that  
23 are often intractable in gain/loss of function studies. Elucidating the master regulatory ar-  
24 chitecture controlling EMT therefore requires inclusion of these complex overlapping and  
25 non-binary behaviors.

26 Systems biology and mathematical modeling are essential tools for understanding  
27 complex developmental programs like EMT (Ahmed & Nawshad, 2007). Previous com-  
28 putational models of TGF- $\beta$  induced differentiation focused on single biological factors or  
29 EMT in single cells. For example, Chung *et al.*, constructed a model of TGF- $\beta$  receptor  
30 activation and Smad signaling using ordinary differential equations and mass-action ki-  
31 netics. Their model suggested that a reduction of functional TGF- $\beta$  receptors in cancer  
32 cells may lead to an attenuated Smad2 signal (Chung *et al.*, 2009). Similarly, Vilar *et al.*  
33 suggested that specific changes in receptor trafficking patterns could lead to phenotypes  
34 that favor tumorigenesis (Vilar *et al.*, 2006). Although these models provided insight into  
35 the role of receptor dynamics, EMT induction involves many other components, includ-  
36 ing competing second messengers and interconnected transcriptional regulatory loops.  
37 Integrating these additional scales of molecular signaling while maintaining the capacity

38 for robust prediction requires a new and expanded computational and experimental strat-  
39 egy. Data-driven systems approaches (Cirit & Haugh, 2012) or logical model formulations  
40 (Morris *et al.*, 2011) are emerging paradigms that constrain model complexity through  
41 the incorporation of training and validation data. These are interesting techniques be-  
42 cause the data informs model structure (which can be expanded as more data becomes  
43 available). Alternatively, Bailey proposed more than a decade ago that a qualitative un-  
44 derstanding of a complex biological system should not require complete definition of its  
45 structural and parametric content (Bailey, 2001). Shortly thereafter, Sethna and cowork-  
46 ers showed that complex model behavior is often controlled by only a few parameter  
47 combinations, a characteristic seemingly universal to multi-parameter models referred  
48 to as “sloppiness” (Machta *et al.*, 2013). Thus, reasonable model predictions are often  
49 possible with only limited parameter information. Taking advantage of this property, we  
50 developed sloppy techniques for parameter identification using ensembles of determin-  
51 istic models (Song *et al.*, 2010). Furthermore, we proposed that the sloppy behavior of  
52 biological networks may also be seen as a source of cell-to-cell (Lequieu *et al.*, 2011) or  
53 even patient-to-patient heterogeneity (Luan *et al.*, 2010). Recently, Bayesian parameter  
54 identification techniques have also been used to explore cell-to-cell heterogeneity (Hase-  
55 nauer *et al.*, 2011, Kalita *et al.*, 2011), where a population of cells could be viewed as a  
56 dynamic ensemble of context-specific biochemical networks (Creixell *et al.*, 2012).

57 In this study, we developed a family of mechanistic models describing the induction  
58 of EMT by TGF- $\beta$  isoforms in the presence and absence of vascular endothelial growth  
59 factor A (VEGF-A). We incorporated mass action kinetics within an ordinary differential  
60 equation (ODE) framework to describe the EMT interaction network containing 97 gene,  
61 protein or mRNA components interconnected through 169 interactions. A family of model  
62 parameters was estimated using 41 molecular data sets generated in DLD1 colon carci-  
63 noma, MDCKII and A375 melanoma cells using the Pareto optimal ensemble technique  
64 (JuPOETs) multiobjective optimization algorithm. JuPOETs generated an ensemble of

65 approximately 1400 models for analysis. Analysis of the model population suggested that  
66 both MCF10A and DLD1 cells could exhibit phenotypic heterogeneity if treated simultane-  
67 ously with TGF- $\beta$ 1/2 and VEGF-A. This heterogeneity was characterized by a significant  
68 fraction of the population being in a “hybrid state” having both high E-cadherin and high  
69 Vimentin expression. We tested these predictions using qRT-PCR and flow-cytometry  
70 studies in a variety of experimental conditions. Validation studies confirmed that upwards  
71 of 45% of the cellular population could be put into the hybrid state in the presence of both  
72 TGF- $\beta$ 1/2 and VEGF-A. Moreover, this response depended upon both activation of Sp1  
73 by MAPK and NFATc1 transcriptional activity consistent with the predicted molecular sig-  
74 naling. Lastly, the hybrid populations of both DLD1 and MCF10A cells exhibited different  
75 functional behavior than those from either TGF- $\beta$  or VEGF-A treatment. The extent of  
76 ductal branch formation significantly increased with MCF10A cells in the hybrid pheno-  
77 type, compared with cells treated with VEGF-A alone. Together, these results establish  
78 a predictive mechanistic model of EMT susceptibility, and reveal a novel signaling axis,  
79 which possibly regulates carcinoma progression through an EMT versus tubulogenesis  
80 response.

81 **Results**

82 **The model population captured key features of TGF- $\beta$  induced EMT** The EMT model  
83 architecture, based upon curated molecular connectivity, described the expression of 23  
84 genes following exposure to TGF- $\beta$  isoforms and VEGF-A (Fig. 1). The EMT model con-  
85 tained 74 molecular species interconnected by 169 interactions. Model equations were  
86 formulated using either saturation or mass-action kinetics within an ordinary differential  
87 equation (ODE) framework. ODEs and mass action kinetics are common tools to model  
88 biochemical pathways (Chen *et al.*, 2009, Schoeberl *et al.*, 2002, Tasseff *et al.*, 2011).  
89 However, while ODE models can simulate complex intracellular behavior, they require es-  
90 timates for model parameters which are often difficult to obtain. The EMT model had 251  
91 unknown model parameters, 169 kinetic constants and 45 non-zero initial conditions. As  
92 expected, these parameters were not uniquely identifiable given the training data (Gad-  
93 kar *et al.*, 2005). Thus, instead of identifying a single best fit (but uncertain) model, we  
94 estimated a sloppy population of models (each consistent with the training data) by simul-  
95 taneously minimizing the difference between model simulations and 41 molecular data  
96 sets using the Pareto Optimal Ensemble Technique (JuPOETs). The training data were  
97 generated in DLD1 colon carcinoma, MDCKII, and A375 melanoma cells following ex-  
98 posure to TGF- $\beta$  isoforms (Medici *et al.*, 2008). We organized these data sets into 11  
99 objective functions which were simultaneously minimized by JuPOETs. Additionally, we  
100 used 12 molecular data sets generated in HK-2 cells following VEGF-A exposure to train  
101 VEGF-A responsive model processes (Lian *et al.*, 2011). To guard against overfitting,  
102 we augmented the multiobjective optimization with leave-one-out cross validation to in-  
103 dependently estimate both the training and prediction error for each objective. Thus, we  
104 generated 11 different model ensembles. Lastly, we compared model predictions with in-  
105 dependent data sets not used during training (both at the molecular and model population  
106 levels) to evaluate the predictive power of the parameter ensemble.

107 JuPOETs generated a population of probable signaling models which captured the

multiple phases of EMT induction (Fig. 2). JuPOETs sampled well over  $10^4$  probable models during each stage of the cross-validation using global random sampling. From this analysis,  $N \simeq 1400$  models were selected for further analysis. The selected models all had the same possible molecular connectivity, but different values for model parameters. Transcription and translation rates, as well as mRNA and protein degradation terms, were set using physical values from the literature (Milo *et al.*, 2010), and allowed to vary by a scaling factor, see methods. Model selection was based upon Pareto rank, the prediction and training error across all objectives. The model population recapitulated key signaling events following TGF- $\beta$  exposure. We subdivided the response to TGF- $\beta$  exposure into two phases. First, TGF- $\beta$ 1/2 signaling initiated a program which downregulated E-cadherin expression in a MAPK dependent manner while simultaneously upregulating TGF- $\beta$ 3 expression. Second, TGF- $\beta$ 3 secretion initiated an autocrine feedback which upregulated the expression of mesenchymal markers such as Vimentin and key upstream transcription factors such as LEF-1 in a SMAD dependent manner. TGF- $\beta$ 3 expression was also able to sustain  $\beta$ -catenin release by inhibiting its sequestration by the APC complex through PI3K mediated GSK3, which was captured by the model (Fig. 4B). Each phase involved the hierachal expression and/or post-translational modification of several key transcription factors. During the first phase, stimulation with TGF- $\beta$ 1/2 (10 a.u.) activated both the SMAD and MAPK pathways. MAPK activation resulted in the phosphorylation of the transcription factor activator protein 1 (AP-1), which in-turn upregulated the expression of Snail, a well established transcriptional repressor (Fig. 2A). Snail expression was MAPK-dependent; the MEK inhibitor U0126 blocked AP-1 activation and Snail expression following TGF- $\beta$ 1/2 exposure (Fig. 2A, Lane 3). Similar results were obtained for Slug expression, confirming initial activation through the MAPK pathway (data not shown). Overexpression of either Snail or Slug upregulated TGF- $\beta$ 3 expression (Fig. 2C) while simultaneously downregulating E-cadherin expression (Fig. 2F). During the second phase, TGF- $\beta$ 3 secretion and the subsequent autocrine signaling resulted in the

135 upregulation of mesenchymal marker expression. The TGF- $\beta$ 3 induced gene expres-  
136 sion program involves a complex hierarchy of transcriptional and post-translational reg-  
137 ulatory events. Absence of E-cadherin indirectly promoted TGF- $\beta$ 3 expression through  
138 the  $\beta$ -catenin/TCF4 complex following Snail or Slug expression (Fig. 2C, Lane 2 or 3).  
139 Conversely, over-expression of E-cadherin inhibited the TGF- $\beta$ 3 autocrine production by  
140 sequestering cytosolic  $\beta$ -catenin, thereby blocking EMT (Fig. 2C, Lane 4 or 5). TGF- $\beta$ 3  
141 signaled through the Smad pathway to regulate LEF-1 expression and downstream tar-  
142 get EMT genes (Fig. 2G). TGF- $\beta$ 3 (10 a.u.) in combination with downstream inhibitors  
143 (DN-Smad4 and DN-LEF-1) completely inhibited Vimentin expression, while elevating E-  
144 cadherin expression (Fig. 2H,I).

145 The predictive power of the ensemble was tested using both cross validation and by  
146 comparing simulations with data sets not used for model training. In whole, 100% of our  
147 training objectives were statistically significant (at a 95% confidence interval) compared  
148 to a randomized parameter family ( $N = 100$ ) generated from a random starting point.  
149 Conversely, we *predicted* 100% of the training objectives, at a 95% confidence interval  
150 compared to randomized parameters (Wicoxon non-parametric test). The model also cap-  
151 tured the temporal gene expression responses of E-cadherin, pSmad2, and LEF-1 (not  
152 used for model training) to within one-standard deviation (up to the 48 hr time-point) (Fig.  
153 2J-L). Taken together, the model captured the key signaling events revealed by Medici *et*  
154 *al.* (Medici *et al.*, 2008) that drive the phenotypic conversion. A listing of objective function  
155 values resulting from training, cross validation and the random parameter control is given  
156 in the supplement (Fig. S1).

157 **Identification of a novel LEF-1 regulator** During model identification, we found that  
158 consistent TGF- $\beta$  induced EMT from a stable epithelial cell population required an addi-  
159 tional regulatory protein. This protein, which we called hypothetical regulator 1 (YREG1),  
160 was required to mediate between SNAIL/SLUG transcriptional activity and the upregu-  
161 lation of LEF-1 expression following TGF- $\beta$ 1/2 exposure. SNAIL/SLUG are well known

transcriptional repressors (Dhasarathy *et al.*, 2011, Hemavathy *et al.*, 2000a,b), although there are a few studies which suggest that at least SNAIL can also act as a transcriptional activator (Guaita *et al.*, 2002). In the model, we assumed the expression of SNAIL/SLUG was likely regulated by AP1/SP1 (Jackstadt *et al.*, 2013). Thus, upon receiving direct SNAIL/SLUG and TGF- $\beta$ 3 signals, the model predicted enhanced SNAIL/SLUG expression, consistent with experimental observations. TGF- $\beta$ 1/2 stimulation also induces LEF-1 expression. However, literature evidence suggested that LEF-1 expression was not strongly dependent upon AP1/SP1 activity (Eastman & Grosschedl, 1999). Thus, either SNAIL/SLUG are acting as inducers (contrary to substantial biochemical evidence) or, they are repressing the expression of an intermediate repressor. Given the biochemical evidence supporting SNAIL/SLUG as repressors, we created the hypothetical YREG1 repressor whose expression is downregulated by SNAIL/SLUG. The literature data therefore suggested that YREG1 had two transcriptional targets, LEF-1 and TGF- $\beta$ 3. By adding this regulator, our simulations became consistent with training and literature data. Medici *et al.* suggested that feedback between  $\beta$ -catenin and LEF-1 was likely, although this feedback had yet to be identified (Medici *et al.*, 2008). Low levels of YREG1 expression were present in all simulations to regulate the formation of the  $\beta$ -catenin-LEF-1 complex. To test the effect of YREG1 on the epithelial population, we conducted over-expression and knockdown simulations on untreated cells (Fig. 4C and 4D). In the absence of YREG1, the population of models failed to consistently retain a stable epithelial state (Fig. 4D). Conversely, YREG1 amplification revealed an enhanced epithelial phenotype, while some inherently transformed cells moved towards a hybrid phenotype (Fig. 4C). Elevated YREG1 repressed LEF-1 and TGF- $\beta$ 3 expression, thereby not allowing free  $\beta$ -catenin to form the  $\beta$ -catenin-LEF-1 complex, or TGF- $\beta$ 3 induced SMAD activation. Taken together, low YREG1 expression was required for the maintenance of a stable epithelial phenotype that was simultaneously inducible across TGF- $\beta$ 1/2, TGF- $\beta$ 3 and SNAIL/SLUG transfection, as seen in the training objectives.

189 **TGF- $\beta$ 1/2 and VEGF-A exposure promotes phenotype heterogeneity through NFATc  
190 and phosphorylated Sp1** While we captured the central tendency of many of the molec-  
191 ular features of EMT induction following TGF- $\beta$ 1/2 exposure, an often neglected but im-  
192 portant emergent feature of developmental and pathological programs is population het-  
193 erogeneity (Park *et al.*, 2010). We (and others) have previously hypothesized that deter-  
194 ministic model ensembles can simulate population behavior, at least at a course grained  
195 level (Lequieu *et al.*, 2011). We tested this hypothesis by analyzing the response of the  
196 population of EMT models to extracellular cues and then comparing this response to flow  
197 cytometry studies. We quantified the phenotypic response of the individual members of  
198 the ensemble to TGF- $\beta$ 1/2 stimulation for two downstream phenotypic markers, Vimentin  
199 (mesenchymal) and E-cadherin (epithelial) following the addition of TGF- $\beta$ 1/2 alone (Fig.  
200 3), and/or VEGF-A in combination with NFATc inhibitors (Fig. 3).

201 We identified model subpopulations that exhibited different behaviors following expo-  
202 sure to TGF- $\beta$ 1/2 (Fig. 3B). Analysis of the molecular signatures of these subpopulations  
203 suggested the abundance, localization and state of the Sp1, AP-1 and NFATc transcription  
204 factors controlled population heterogeneity. The majority of models (>80%) responded to  
205 treatment, moving away from the untreated population (Fig 3A-C, gray). These mod-  
206 els showed the classically expected behavior, a switch from an epithelial to mesenchy-  
207 mal phenotype following TGF- $\beta$ 1/2 exposure. Some models resembled untreated cells;  
208 they had elevated nuclear localized phosphorylated Sp1, relative to non-induced cells,  
209 which decreased E-cadherin expression through Slug-mediated inhibition, which in turn  
210 increased Vimentin expression through TGF- $\beta$ 3 autocrine signaling and the liberation  
211 of  $\beta$ -catenin. However, the most biologically interesting behavior was exhibited by cells  
212 achieving a hybrid phenotype, most notable in a dual treatment condition (3C, black ar-  
213 row), but also present in a small percentage of untreated cells (Fig. 3A). Models with this  
214 hybrid phenotype had elevated Sp1 and NFAT transcriptional activity, resulting in simulta-  
215 neously increased Vimentin and E-cadherin expression (Fig. 4A).

216 To better understand the hybrid phenotype, we simulated the response of the model  
217 population to TGF- $\beta$ 1/2 and VEGF-A treatment with and without NFATc inhibitors (Fig.  
218 3). As expected, stimulation with VEGF-A (50 a.u.) maintained an epithelial population  
219 (Fig. 3A), while TGF- $\beta$ 1/2 (10 a.u.) exposure shifted the population from an epithelial  
220 to a mesenchymal phenotype (Fig. 3B). On the other hand, combined stimulation with  
221 TGF- $\beta$ 1/2 (10 a.u.) and VEGF-A (50 a.u.) increased both E-cadherin and Vimentin ex-  
222 pression, resulting in a hybrid phenotype with both epithelial and mesenchymal character-  
223 istics (Fig. 3C). Vimentin expression was correlated with high levels of nuclear phospho-  
224 rylated Sp1, following TGF- $\beta$ 1/2 exposure. Conversely, elevated E-cadherin expression  
225 depended upon the activity of NFAT transcription factors downstream of VEGF-A stimula-  
226 tion. To further isolate the role of NFAT on this hybrid state, we simulated the inhibition of  
227 NFAT transcriptional activity across all conditions (all else being equal). NFAT inhibition  
228 in combination with VEGF-A or TGF- $\beta$ 1/2 treatments blocked increased E-cadherin ex-  
229 pression in the case of VEGF-A (Fig. 3D), but did not influence TGF- $\beta$ 1/2 signaling (Fig.  
230 3E). Lastly, NFATc inhibition in combination with simultaneous TGF- $\beta$ 1/2 and VEGF-A  
231 exposure repressed nearly all E-cadherin expression, shifting nearly the entire population  
232 towards a mesenchymal phenotype (Fig. 3F). Taken together, high levels of nuclear local-  
233 ized phosphorylated Sp1 correlated with Vimentin expression, while NFATc transcriptional  
234 activity was critical for maintaining E-cadherin expression in the presence of competing  
235 signals.

236 **Combined TGF- $\beta$ 2 and VEGF-A exposure drives heterogeneity in MCF10A and**  
237 **DLD1 cells** The EMT model simulations suggested the transcriptional activity of NFATc  
238 and Sp1 could be independently tuned to generate a hybrid cell population with both  
239 epithelial and mesenchymal characteristics. To test this hypothesis, we exposed either  
240 quiescent epithelial (MCFA10, (Fig. 5)) or transformed epithelial cells (DLD1, (Fig. S2))  
241 to combinations of TGF- $\beta$ 1/2 and/or VEGF-A. As expected, treatment with TGF- $\beta$ 1/2  
242 (10ng/ml) increased Slug and Vimentin expression, while repressing E-cadherin expres-

sion both at the transcript and protein levels in MCF10A (Fig. 5A-B) and DLD1 cells (Fig. S3C, Fig S3 D,E). Both MCF10A (Fig. 5C) and DLD1 cells (Fig. S2E,G) transitioned from quiescent cobblestone morphology to spread spindle shapes, consistent with EMT. As predicted, we found increased nuclear localization of phosphorylated Sp1 following TGF- $\beta$ 1/2 stimulation in both MCF10A (Fig. 5B,C) and DLD1 cells (Fig. S2E,F). Consistent with model predictions, VEGF-A (50ng/ml) treatment increased the abundance of NFATc1 and E-cadherin at both the transcript and protein level in both MCF10A (Fig. 5A) and DLD1 (Fig. S2A) cells. We also found that NFATc1 nuclear localization significantly increased in both MCF10 and DLD1 treated with VEGF-A independently of the abundance of nuclear localized phosphorylated Sp1 levels (Fig. 5B,C Fig.S3C,E ). Interestingly, combining VEGF-A (50ng/ml) with TGF- $\beta$ 1/2 (10ng/ml) resulted in significantly elevated expression of both E-cadherin and Vimentin at the transcript and protein levels in both MCF10A and DLD1 cells (Fig 5A,B; Fig S3D,E; Fig S4C). NFATc1 expression increased, while Sp1 expression was similar to the TGF- $\beta$ 1/2 case alone (Fig. 5A-B, Fig S3D,E; Fig S4C)), supporting their independent regulation. The expression of Slug, and Vimentin significantly increased, while E-cadherin levels were increased in MCF10A cells (Fig 5A) and maintained at control levels in DLD1 cells (Fig. S3D). As further predicted, nuclear co-localization of both NFATc1 and phosphorylated Sp1 were apparent in MCF10A and DLD1 cells treated with both ligands (Fig. 5B,C Fig S3E,F). Taken together, combined VEGF-A and TGF- $\beta$ 1/2 treatment elicited a hybrid phenotype expressing both mesenchymal and epithelial characteristics in both MCF10A and DLD1 cells. This phenotype was driven by the transcriptional activity of two key transcription factors, Sp1 and NFATc, which could be modulated independently by TGF- $\beta$ 1/2 and VEGF-A exposure.

Our phenotypic analysis predicted that NFATc transcriptional activity was critical to maintaining E-cadherin expression in the presence of both VEGF-A and TGF- $\beta$ 1/2. We experimentally tested this hypothesis by exposing both MCF10A (Fig. 5E,F) and DLD1 cells (Fig. S3) to combinations of VEGF-A and TGF- $\beta$ 1/2 in the presence or absence

270 of VIVIT, a soluble peptide inhibitor of NFATc transcriptional activity (Aramburu *et al.*,  
271 1999). Treatment with VEGF-A (50ng/ml) and VIVIT (10 $\mu$ M) in MCF10A cells significantly  
272 reduced E-cadherin expression compared to VEGF-A alone (Fig 5D,E). Co-treatment  
273 with VIVIT and TGF- $\beta$ 1/2 did not enhance EMT capacity of MCF10A cells above that  
274 of TGF- $\beta$ 1/2 alone (Fig 5A,B,E). Likewise, VIVIT in combination with both TGF- $\beta$ 1/2  
275 and VEGF-A resulted in a loss of E-cadherin gene and protein expression, while Slug  
276 and Vimentin levels remained increased (Fig. 5D,E ). Quantitative flow cytometry con-  
277 firmed these results in both MCF10A (Fig. 5F) and DLD1 cells (Fig. S4C). Both epithelial  
278 cell lines initially had high levels of E-cadherin expression, and low vimentin abundance  
279 (Q1-99.5%), but both MCF10A and DLD1 cells shifted from an epithelial to mesenchymal  
280 phenotype (Q1-33.4%, Q4-42.8%) following TGF- $\beta$ 1/2 exposure. As expected, NFATc  
281 nuclear localization was repressed with VIVIT treatment regardless of ligand stimulation,  
282 while the abundance of nuclear phosphorylated Sp1 increased for both TGF- $\beta$ 1/2 and  
283 TGF- $\beta$ 1/2 + VIVIT conditions (Fig. 5D,E). Combined TGF- $\beta$ 1/2 and VEGF-A increased  
284 both Vimentin and E-cadherin expression (Q1-42.1%, Q2-52.3%) compared to TGF- $\beta$ 1/2  
285 alone. Together, these results demonstrate that NFATc and phosphorylated Sp1 are criti-  
286 cal for regulating E-cadherin and Vimentin expression during phenotype heterogeneity in  
287 MCF10A and DLD1.

288 **Ductal branching during acini formation is dependent upon phenotype heterogene-  
289 ity in MCF10A and DLD1 cells** We finally employed established three-dimensional  
290 (3D) *in vitro* models of invasion, migration, compaction, and tubulogenesis (Dhimolea  
291 *et al.*, 2010) to determine the functional consequences of the hybrid phenotype (Fig. 6).  
292 MCF10A and DLD1 cells were aggregated via hanging drop, placed on the surface of a  
293 collagen gel, and cultured for 72 hrs under various biochemical treatments. TGF- $\beta$ 1/2  
294 stimulation significantly enhanced cell matrix invasion and matrix compaction, while in  
295 contrast VEGF-A stimulation promoted surface migration but no invasion or compaction  
296 (Fig. 6B-D). Interestingly, combined TGF- $\beta$ 1/2 and VEGF-A stimulation significantly in-

297 creased cell migration potential above that of VEGF-A alone while maintaining 3D matrix  
298 compaction, though with decreased magnitude compared to TGF- $\beta$ 1/2 alone. Inhibi-  
299 tion of NFATc transcriptional activity by VIVIT decreased migration following treatment  
300 with VEGF-A alone (Fig. 6B). Co-treatment of VIVIT significantly decreased migration,  
301 while complementarily increasing invasion and compaction, when MCF10A cells were  
302 stimulated with both VEGF-A and TGF- $\beta$ 1/2 (Fig. 6B-D). The responses of DLD1 cells  
303 followed a similar trend to MCF10A, although the magnitudes of migration, invasion, and  
304 compaction were less. Cell circularity within 3D gels strongly and negatively correlated  
305 with both invasion and compaction regardless of treatment (Fig. 6E). Circular-  
306 ity index, a common means of quantifying cell morphology, relates cell area to perimeter.  
307 A perfect circle has a circularity index equal to 1.0, while a straight line has a circularity  
308 index equal to 0.0, see Butcher et al. (Butcher *et al.*, 2004). TGF- $\beta$ 1/2 treatment alone  
309 resulted in irregular and spindle shaped morphology, while VEGF-A exposure promoted  
310 round quiescent cells (Fig. 6A). Combined VEGF-A and TGF- $\beta$ 1/2 promoted morphology  
311 between these extremes. VIVIT mediated NFATc inhibition significantly reduced the cir-  
312 cularity index, similar to TGF- $\beta$ 1/2 treatment (Fig. 6F). VEGF-A treatment also induced  
313 the formation of tubular structures (acini), but the number of tubular branches relative to  
314 total acini was significantly increased upon combined TGF- $\beta$ 1/2 and VEGF-A. No tubular  
315 structures were identified within the DLD1 constructs during the 7 day tubulogenesis end-  
316 points, supporting that MCF10A and DLD1 cells have some cell-type specific EMT sensi-  
317 tivity despite their underlying competency for acquiring a heterogeneous phenotype. This  
318 suggests that initial EMT sensitivity of a cell influences downstream functional response  
319 from TGF- $\beta$  and VEGFA stimulation. Together, these results establish that VEGF-A and  
320 TGF- $\beta$ 1/2 ligand concentrations potentiate between acini and ductal branch formation in  
321 3D culture, and are dependent upon NFATc activity.

324 **Discussion**

325 In this study, we developed a family of mechanistic models describing the induction of  
326 EMT by TGF- $\beta$  isoforms in the presence and absence of VEGF-A. The signaling architec-  
327 ture encoded in the model, which contained 74 molecular species interconnected by 169  
328 interactions, described the expression of 23 genes in response to growth factor stimula-  
329 tion. This simulation incorporates an unprecedented level of detail compared to previous  
330 models, but as a consequence created a large number of unknown model parameters.  
331 Because these parameters could not be estimated uniquely apriori, we estimated an en-  
332 semble of likely parameters using the JuPOETs multiobjective optimization framework.  
333 The model population was trained and cross-validated to prescribe biological significance  
334 using 41 data sets generated in DLD1 colon carcinoma, MDCKII, and A375 melanoma  
335 cell lines (Medici *et al.*, 2008). The absence of TGF- $\beta$ 1/2 or VEGF-A stimulation was  
336 used as the baseline for the robustness calculations. Analysis of this population pre-  
337 dicted possible phenotypic modes (and their associated signaling) that cells could exhibit  
338 when stimulated with TGF- $\beta$  and/or VEGF-A. The most novel hypothesis generated from  
339 the analysis was that cells could operate in a hybrid state defined by both epithelial and  
340 mesenchymal traits when stimulated simultaneously with TGF- $\beta$  and VEGF-A. We tested  
341 this hypothesis in MCF10A and DLD1 cells stimulated with combinations of TGF- $\beta$  and  
342 VEGF-A. As expected, in the presence of TGF- $\beta$  or VEGF-A alone, MCF10A and DLD1  
343 cells were either mesenchymal or epithelial, respectively. However, with both TGF- $\beta$  and  
344 VEGF-A, MCF10A and DLD1 cells exhibited a hybrid phenotype, having both epithe-  
345 lial and mesenchymal characteristics. Furthermore, we found that functional traits such  
346 as tubulogenesis and ductal branching were different for cells in this hybrid phenotype.  
347 Together, this study established a predictive model of EMT induction, determined that  
348 deterministic model ensembles could predict population heterogeneity, and proved the  
349 existence of a unique hybrid phenotype resulting from the simultaneous integration of  
350 extracellular growth factor signals.

351 Cells routinely process a multitude of signals simultaneously, especially when coordi-  
352 nating developmental or pathological programs. For example, oncogenic cells integrate  
353 both mechanical and chemical cues in their local microenvironment during tumorigenesis,  
354 including cytokines VEGF and TGF- $\beta$  (Hong *et al.*, 2013). VEGF-A mediates patholog-  
355 ical angiogenic remodeling of tumors (Nagy *et al.*, 2007), while TGF- $\beta$  can elicit both  
356 protective and oncogenic responses (Ferrara, 2002, Willis & Borok, 2007). While much  
357 research has tested signaling pathways individually, far less is understood about com-  
358 binatorial stimulation, such as with both VEGF-A and TGF- $\beta$ . Recent *in vitro* and *in*  
359 *vivo* evidence has suggested that epithelial cells can exhibit heterogeneous phenotypes  
360 in addition to classically defined epithelial or mesenchymal states (Polyak & Weinberg,  
361 2009, Strauss *et al.*, 2011). For example, expression profiling in human epithelial cancer  
362 cell lines demonstrated a spectrum of phenotypes, including some that expressed both  
363 E-cadherin and Vimentin simultaneously (Neve *et al.*, 2006, Welch-Reardon *et al.*, 2014).  
364 Zajchowski *et al.*, speculated that these expression profiles were somehow important for  
365 maintaining epithelial properties, while simultaneously allowing other functional behavior  
366 such as proliferation and migration (Zajchowski *et al.*, 2001). Whether and how heteroge-  
367 neous phenotypes arise and participate in cancer progression, as well as their response  
368 to pharmacological inhibition are fundamental questions that should receive increased at-  
369 tention. In this study, we determined that a hybrid phenotype could be obtained through  
370 combined treatment with VEGF-A and TGF- $\beta$ , both common factors localized in the tu-  
371 mor microenvironment. Furthermore, our systematic simulation-experimentation strategy  
372 identified that the transcriptional activity of Sp1 and NFATc were the critical factors con-  
373 trolling this phenotypic heterogeneity. Several studies have highlighted the importance  
374 of NFATc as a key transcription factor involved in cell growth, survival, invasion, angio-  
375 genesis and cancer (Mancini & Toker, 2009). For example, proliferation and anchorage-  
376 independent growth of pancreatic tumor cells is dependent on calcineurin and NFATc1  
377 activity, consistent with the high levels of nuclear NFATc1 found in pancreatic tumors

378 (Singh *et al.*, 2010). Likewise, our results found that VEGF-A was a potent inducer of  
379 NFATc1 expression, which may be required for epithelial cell migration and tubulogenesis.  
380 Although specific NFATc isoforms were not distinguished in the model, our simulations  
381 suggested that NFATc transcriptional activity was capable of maintaining epithelial traits,  
382 even during TGF- $\beta$  induced EMT. Experimentally, we found that E-cadherin expression  
383 was dependent upon NFATc dephosphorylation in response to simultaneous VEGF-A and  
384 TGF- $\beta$ 1/2 treatment. Thus, these results support the hypothesis that NFATc activity plays  
385 a critical role in maintaining cell-cell contacts, even during partial EMT.

386       Epithelial cells reproduce tissue-like organization when grown in a three-dimensional  
387 extracellular matrix (ECM) environment, and therefore are an attractive model to study  
388 morphogenic mechanisms. It is well established that MCF10A cells form structures that  
389 closely resemble acini (multi-lobed cluster of cells) in three-dimensional *in vitro* cultures  
390 (Debnath *et al.*, 2003). It has been postulated that a cellular response reminiscent of  
391 partial EMT underlies this process, stimulating further branching and formation of acini  
392 (Pearson & Hunter, 2007). Normally well controlled process such as tubulogenesis can  
393 be co-opted by cancer cells to break away from a primary lesion and invade through  
394 the surrounding stroma (O'Brien *et al.*, 2004). However, by retaining a transient hybrid  
395 EMT-like state, clusters of these tube-forming tumor cells can reform at a high rate af-  
396 ter invasion, possibly explaining why invasive human carcinomas frequently appear to be  
397 cellular collections with varying degrees of gland-like differentiation (Debnath & Brugge,  
398 2005). In this study, we showed that our predicted hybrid phenotype generated by sim-  
399 taneous treatment of epithelial cells with VEGF-A and TGF- $\beta$  possessed altered migra-  
400 tion and invasion, which enhanced tubular branching. A salient feature of this behavior,  
401 however, was the retention of cell-cell contacts that allowed cells to migrate without com-  
402 pletely dissociating from their neighbors. Thus, our results support a mechanism in which  
403 hybrid cells can maintain some functional characteristics of epithelial cells such as cell-  
404 cell adhesion, which are normally lost in a fully differentiated mesenchymal state. The

tumor microenvironment contains many soluble signals simultaneously, including VEGF and TGF- $\beta$ . Thus, it is likely that some cancerous epithelial cells could exhibit hybrid EMT phenotypic states. This may explain why fibroblastoid morphology, a classical feature of EMT, is not commonly observed in human carcinomas (Debnath & Brugge, 2005). This study focused on the combinatorial effects of two very different ligand families present together in the tumor environment. Additional modeling studies are required to unravel the global response of epithelial cells to the full spectrum of chemical, substrate, and mechanical cues. The simulation strategy presented here is readily adaptable to larger species sets, with the major advantage that experimentally testable hypotheses can be generated regarding how signals get integrated to produce global cellular response. Furthermore, by simulating multiple ensembles of parameter sets, subpopulations across a constellation of phenotypes can be created and mined for common and/or divergent signaling characteristics. This is a significant advantage over forced convergence to a single unique solution and thereby generating a potentially non-physiological homogeneous population.

The deterministic population of EMT models predicted heterogeneous behavior that was qualitatively consistent with experimental studies. There is a diversity of algorithmic approaches to estimate model parameters (Moles *et al.*, 2003), as well as many strategies to integrate model identification with experimental design (Rodriguez-Fernandez *et al.*, 2013, Villaverde & Banga, 2014). However, despite these advances, the identification of models describing intracellular network behavior remains challenging. There are different schools of thought to deal with this challenge. One school has focused on model reduction. Data-driven approaches (Cirit & Haugh, 2012), boolean (Choi *et al.*, 2012) or other logical model formulations (Morris *et al.*, 2011, Terfve *et al.*, 2012) are emerging paradigms that constrain model complexity by the availability of the training and validation data. Other techniques such as constraints based modeling, which is commonly used to model metabolic networks, have also been applied to model transcriptional networks, although primarily in lower eukaryotes and prokaryotes (Hyduke & Palsson, 2010). These

432 techniques (and many others, see review (Wayman & Varner, 2013)) are certainly ex-  
433 citing, with many interesting properties. However, we used the traditional approach of  
434 mass action kinetics within an ordinary differential equation framework. The identifica-  
435 tion problem for the EMT model was massively underdetermined. This is not uncommon  
436 for differential equation models, especially those that are highly mechanistic. Of course,  
437 we could have discarded mechanism or reduced the model scope to decrease the com-  
438 plexity of the identification problem. However, a central criticism leveled by biologists is  
439 that model simplification is often done at the cost of biological reality, or done for reasons  
440 of computational expediency (Sainani, 2012). To avoid this criticism, we systematically  
441 identified an ensemble of likely models each consistent with the training data, instead of a  
442 single but uncertain best fit model. Previously, we (and others) have suggested that deter-  
443 ministic ensembles could model heterogeneous populations in situations where stochastic  
444 computation was not feasible (Lequieu *et al.*, 2011). Population heterogeneity using deter-  
445 ministic model families has previously been explored for bacterial growth in batch cultures  
446 (Lee *et al.*, 2009). In that case, distributions were generated because the model parame-  
447 ters varied over the ensemble, i.e., extrinsic noise led to population heterogeneity. In this  
448 study, parameters controlling physical interactions such as disassociation rates or the rate  
449 of assembly or degradation of macromolecular machinery such as ribosomes were widely  
450 distributed over the ensemble. Population heterogeneity can also arise from intrinsic ther-  
451 mal fluctuations, which are not captured by a deterministic population of models (Swain  
452 *et al.*, 2002). Thus, deterministic ensembles, provide a coarse-grained or extrinsic-only  
453 ability to simulate population diversity. Despite this limitation, our prediction of phenotypic  
454 heterogeneity (and the underlying signaling events responsible for the heterogeneity) was  
455 consistent with experimental observations. This suggested that deterministic ensembles  
456 could simulate disease or developmental processes in which heterogeneity plays an im-  
457 portant role, without having to resort to stochastic simulation.

458 A common criticism of ODE modeling has been the poorly characterized effect of

459 structural and parametric uncertainty. In this study, parametric uncertainty was addressed  
460 by developing an ensemble of probable models instead of a single best-fit but uncertain  
461 model using multiobjective optimization. While computationally complex, multiobjective  
462 optimization is an important tool to address qualitative conflicts in training data that arise  
463 from experimental error or cell line artifacts (Handl *et al.*, 2007). On the other hand, struc-  
464 tural uncertainty is defined as uncertainty in the biological connectivity. The EMT model  
465 connectivity was assembled from an extensive literature review. However, several poten-  
466 tially important signaling mechanisms were not included. First, we identified a potential  
467 gap in biological knowledge surrounding the regulation of LEF-1 expression, that was filled  
468 by the addition of the hypothetical YREG1 transcriptional repressor. The LEF-1 transcrip-  
469 tion factor is expressed in tissues that undergo EMT during embryogenesis (Nawshad &  
470 Hay, 2003, Vega *et al.*, 2004), and has been suggested to promote an invasive phenotype  
471 in cancer cells (Cano *et al.*, 2000, Kim *et al.*, 2002). Low levels of YREG1 were important  
472 for stabilizing the interaction between LEF-1 and  $\beta$ -catenin, while elevated levels inhibited  
473 EMT by downregulating LEF-1 transcriptional activity. Recent evidence has established a  
474 complex role of Amino terminal Enhancer of Split (AES) and Groucho/TLE on suppress-  
475 ing LEF-1 activity. AES opposes LEF-1 transcriptional activation while Groucho/TLE binds  
476 with LEF-1 for a histone deacetylase repression. In addition,  $\beta$ -catenin directly displaces  
477 Groucho/TLE repressors from TCF/LEF-1 in Wnt-mediated transcription activation (Arce  
478 *et al.*, 2009, Grumolato *et al.*, 2013). Our model agrees with this newly discovered feed-  
479 back system, as YREG1 regulates LEF-1 activity leading to EMT stabilization.

480       Recent evidence has also suggested an essential role of NF- $\kappa$ B in epithelial trans-  
481 formation. NF- $\kappa$ B may influence Snail expression through the AKT pathway and directly  
482 stabilize Snail activity (Wu *et al.*, 2009). This is particularly important for integrating in-  
483 flammation pathways, such as interleukin-6 (IL-6) and tumor necrosis factor- $\alpha$  (TNF- $\alpha$ ),  
484 which have been linked to EMT in pathological conditions (Sullivan *et al.*, 2009). Other  
485 pathways such as Notch have also been shown to act synergistically with TGF- $\beta$  to ex-

486 press Slug in the developing embryo (Niessen *et al.*, 2008). Lastly, while we have modeled  
487 classical protein signaling, we have not considered the role of regulatory RNAs on EMT.  
488 There is growing evidence that microRNAs (miRNAs) play a strong role in EMT, where  
489 several miRNAs, for example miR-21 and miR-31 are strongly associated with TGF- $\beta$  ex-  
490 posure (Bullock *et al.*, 2012). Addressing missing structural components like these, could  
491 generate more insight into TGF- $\beta$  signaling and its role in phenotypic transformation.

492 **Materials and Methods**

493 The model code and parameter ensemble is freely available under an MIT software li-  
494 cense and can be downloaded from <http://www.varnerlab.org>.

495 **Signaling network connectivity** The EMT model described the gene expression pro-  
496 gram resulting from TGF- $\beta$  and VEGF-A signaling in a prototypical epithelial cell. The  
497 TGF- $\beta$ -EMT network contained 97 nodes (proteins, mRNA or genes) interconnected by  
498 251 interactions. The network connectivity was curated from more than 40 primary liter-  
499 ature sources in combination with on-line databases (Jensen *et al.*, 2009, Linding *et al.*,  
500 2007). The model interactome was not specific to a single epithelial cell line. Rather, we  
501 assembled canonical pathways involved in TGF- $\beta$  and VEGF-A signaling, defaulting to  
502 human connectivity when possible. Using a canonical architecture allowed us to explore  
503 general features of TGF- $\beta$  induced EMT without cell line specific artifacts. On the other  
504 hand, because of the canonical architecture, we can test the model against several cell  
505 lines to test the generality of our conclusions.

506 Our signaling network reconstruction was based on Medici *et al.* who identified the  
507 pathways through which MDCKII, DLD1 colon carcinoma, and A375 melanoma cells tran-  
508 sition towards a mesenchymal phenotype (Medici *et al.*, 2008). Sequential activation of  
509 MAPK and Smad pathways were initiated upon addition of TGF- $\beta$ 1/2. Briefly, TGF- $\beta$ 2  
510 signals through the RAS-RAF-MEK-ERK pathway to up-regulate Snail and Slug expres-  
511 sion (Medici *et al.*, 2006). Snail, a known repressor of junctional proteins, inhibits the ex-  
512 pression of E-cadherin (Cano *et al.*, 2000). This initial repression of E-cadherin leads to a  
513 release of  $\beta$ -catenin from the cell membrane. This release of  $\beta$ -catenin can then translo-  
514 cate to the nucleus and form transcriptional complexes with TCF-4 to drive TGF- $\beta$ 3 ex-  
515 pression (Medici *et al.*, 2008). The PI3K to GSK3 pathway was included and acted as an  
516 activating mechanism of  $\beta$ -catenin signaling through TGF- $\beta$ 3 signaling ,itepMedici:2008fk.  
517 GSK3 is known to act on  $\beta$ -catenin signaling through the ubiquitin-proteasome pathway  
518 (Larue & Bellacosa, 2005, Zhou *et al.*, 2004). Thereby, further  $\beta$ -catenin release also re-

519 sulted from by TGF- $\beta$ 3 signals to the cells interior by binding to type II receptors, which  
520 form heterodimers with type I receptors (ALK5) (Derynck & Zhang, 2003). This activates  
521 the receptors serine/threonine kinase activity to phosphorylate and activate the recep-  
522 tor Smads 2/3 (Massagué *et al.*, 2005). In the model, receptors are represented as either  
523 bound or unbound complexes. Phosphorylated Smads 2/3 (pSmad2/3) form heterodimers  
524 and translocate to the nucleus. pSmads complexes up-regulate other transcription fac-  
525 tors, such as LEF-1. The pSmad2/4-LEF-1 complex has been shown to directly repress  
526 the E-cadherin gene (Nawshad *et al.*, 2007). LEF-1 also binds with  $\beta$ -catenin to upregu-  
527 late mesenchymal proteins such as fibronectin (Medici *et al.*, 2011). In the model, Smad  
528 signaling is lumped into a single smad species that can act in a co-dependent fashion  
529 with LEF1 to downregulate E-cadherin. The EMT gene expression program was initiated  
530 by the binding of TGF- $\beta$  isoforms to TGF- $\beta$  surface receptors. Binding of extracellu-  
531 lar TGF- $\beta$ 1/2 with TGF- $\beta$  surface receptors I/II (TGF- $\beta$ R-I/II) initiates the assembly of  
532 adapter complexes which starts the downstream signaling program. Complex assem-  
533 bly activates the serine/threonine kinase activity on the receptor, leading to the recruit-  
534 ment and phosphorylation of Smad partners (Massagué *et al.*, 2005). Phosphorylated  
535 Smads2/3 (pSmad2/3) form heterodimers with partner Smad4 and then translocate to the  
536 nucleus where they act as both transcriptional activators and repressors. Repression of  
537 E-cadherin expression is the central event in the transition from an epithelial to a mes-  
538 enchymal phenotype (Cano *et al.*, 2000). However, this transition is not solely driven by  
539 transcriptional events. At the protein level, the repression of E-cadherin leads to a release  
540 of  $\beta$ -catenin from cell membrane. Cytosolic  $\beta$ -catenin then translocates to the nucleus and  
541 forms transcriptionally-active complexes with immunoglobulin transcription factor 2 (TCF-  
542 4) to drive TGF- $\beta$ 3 expression (Medici *et al.*, 2008). The PI3K to GSK3 pathway was  
543 included and acted as an activating mechanism of  $\beta$ -catenin signaling through TGF- $\beta$ 3  
544 signaling (Medici *et al.*, 2008). GSK3 is known to act on  $\beta$ -catenin signaling through  
545 the ubiquitin-proteasome pathway. (Larue & Bellacosa, 2005, Zhou *et al.*, 2004). Lastly,

546 VEGF-A activation of NFATc1 takes place through calcineurin signaling leading to an en-  
 547 hancement of E-cadherin expression (Suehiro *et al.*, 2014), as supported by our VEGF-A  
 548 experimental data (Fig. S4).

549 **Formulation, solution and analysis of the EMT model equations**

550 *EMT signaling events.* EMT signaling events were modeled using either saturation or  
 551 mass-action kinetics within an ordinary differential equation (ODE) framework:

$$\frac{1}{\tau_i} \frac{dx_i}{dt} = \sum_{j=1}^{\mathcal{R}} \sigma_{ij} r_j(\mathbf{x}, \epsilon, \mathbf{k}) - \mu x_i \quad i = 1, 2, \dots, \mathcal{M} \quad (1)$$

552 where  $\mathcal{R}$  denotes the number of signaling reactions and  $\mathcal{M}$  denotes the number of pro-  
 553 teins in the model. The quantity  $\tau_i$  denotes a time scale parameter for species  $i$  which  
 554 captures unmodeled effects. In the current study  $\tau_i = 1$  for all species. The quantity  
 555  $r_j(\mathbf{x}, \epsilon, \mathbf{k})$  denotes the rate of reaction  $j$ . Typically, reaction  $j$  is a non-linear function of  
 556 biochemical and enzyme species abundance, as well as unknown model parameters  $\mathbf{k}$   
 557 ( $\mathcal{K} \times 1$ ). The quantity  $\sigma_{ij}$  denotes the stoichiometric coefficient for species  $i$  in reaction  $j$ . If  
 558  $\sigma_{ij} > 0$ , species  $i$  is produced by reaction  $j$ . Conversely, if  $\sigma_{ij} < 0$ , species  $i$  is consumed  
 559 by reaction  $j$ , while  $\sigma_{ij} = 0$  indicates species  $i$  is not connected with reaction  $j$ . Species  
 560 balances were subject to the initial conditions  $\mathbf{x}(t_o) = \mathbf{x}_o$ .

561 Rate processes were written as the product of a kinetic term ( $\bar{r}_j$ ) and a control term ( $v_j$ )  
 562 in the EMT model. The rate of enzyme catalyzed reactions was modeled using saturation  
 563 kinetics:

$$\bar{r}_j = k_j^{cat} \epsilon_i \left( \frac{x_s}{K_{js} + x_s} \right) \quad (2)$$

564 where  $k_j^{cat}$  denotes the catalytic rate constant for reaction  $j$ ,  $\epsilon_i$  denotes the abundance of  
 565 the enzyme catalyzing reaction  $j$ , and  $K_{js}$  denotes the saturation constant for species  $s$   
 566 in reaction  $j$ . On the other hand, mass action kinetics were used to model protein-protein

567 binding interactions within the network:

$$\bar{r}_j = k_j^{\max} \prod_{s \in m_j^-} x_s^{-\sigma_{sj}} \quad (3)$$

568 where  $k_j^{\max}$  denotes the maximum rate for reaction  $j$ ,  $\sigma_{sj}$  denotes the stoichiometric coefficient for species  $s$  in reaction  $j$ , and  $s \in m_j$  denotes the set of *reactants* for reaction  $j$ .

570 We assumed all binding interactions were irreversible.

571 The control terms  $0 \leq v_j \leq 1$  depended upon the combination of factors which influenced rate process  $j$ . For each rate, we used a rule-based approach to select from competing control factors. If rate  $j$  was influenced by  $1, \dots, m$  factors, we modeled this relationship as  $v_j = \mathcal{I}_j(f_{1j}(\cdot), \dots, f_{mj}(\cdot))$  where  $0 \leq f_{ij}(\cdot) \leq 1$  denotes a regulatory transfer function quantifying the influence of factor  $i$  on rate  $j$ . The function  $\mathcal{I}_j(\cdot)$  is an integration rule which maps the output of regulatory transfer functions into a control variable. In this study, we used  $\mathcal{I}_j \in \{\min, \max\}$  (Sagar & Varner, 2015). If a process has no modifying factors,  $v_j = 1$ .

579 *EMT gene expression processes.* The EMT model described both signal transduction  
580 and gene expression events following the addition of TGF- $\beta$  and VEGF-A. For each  
581 gene, we modeled both the resulting mRNA ( $m_j$ ) and protein ( $p_j$ ):

$$\frac{dm_j}{dt} = r_{T,j} - (\mu + \delta_{m,j}) m_j + \lambda_j \quad (4)$$

$$\frac{dp_j}{dt} = r_{X,j} - (\mu + \delta_{p,j}) p_j \quad (5)$$

582 where  $j = 1, 2, \dots, \mathcal{G}$ . The terms  $r_{T,j}$  and  $r_{X,j}$  denote the specific rate of transcription,  
583 and translation while the terms  $\delta_{m,j}$  and  $\delta_{p,j}$  denote degradation constants for mRNA and  
584 protein, respectively. Lastly,  $\mu$  denotes the specific growth rate, and  $\lambda_j$  denotes the con-  
585 stitutive rate of gene expression for gene  $j$ . The specific transcription rate was modeled  
586 as the product of a kinetic term  $\bar{r}_{T,j}$  and a control term  $u_j$  which described how the abun-

587 dance of transcription factors, or other regulators influenced the expression of gene  $j$ .

588 The kinetic rate of transcription was modeled as:

$$\bar{r}_{T,j} = \alpha_j \left[ V_T^{\max} \left( \frac{G_j}{K_T + G_j} \right) \right] \quad (6)$$

589 where the maximum gene expression rate was defined as the product of a character-  
590 istic transcription rate constant ( $k_T$ ) and the abundance of RNA polymerase,  $V_T^{\max} =$   
591  $k_T (RNAP)$ . The parameter  $\alpha_j$  was used to adjust the transcription to that of gene  $j$  (es-  
592 timated in this study), while  $k_T$ ,  $G_j$  and  $RNAP$  were estimated from literature (Milo *et al.*,  
593 2010). Similar to the signaling processes, the gene expression control term  $0 \leq u_j \leq 1$   
594 depended upon the combination of factors which influenced rate process  $j$ . For each  
595 rate, we used a rule-based approach to select from competing control factors. If the ex-  
596 pression of gene  $j$  was influenced by  $1, \dots, m$  factors, we modeled this relationship as  
597  $u_j = \mathcal{I}_j(f_{1j}(\cdot), \dots, f_{mj}(\cdot))$  where  $0 \leq f_{ij}(\cdot) \leq 1$  denotes a regulatory transfer function  
598 quantifying the influence of factor  $i$  on the expression of gene  $j$ . The function  $\mathcal{I}_j(\cdot)$  is an  
599 integration rule which maps the output of regulatory transfer functions into a control vari-  
600 able. In this study, we used  $\mathcal{I}_j \in \{\min, \max\}$  (Sagar & Varner, 2015). If a gene expression  
601 process has no modifying factors,  $u_j = 1$ . Lastly, the specific translation rate was modeled  
602 as:

$$r_{X,j} = \beta_j \left[ V_X^{\max} \left( \frac{m_j}{K_X + m_j} \right) \right] \quad (7)$$

603 where  $V_X^{\max}$  denotes a characteristic maximum translation rate estimated from literature,  
604  $\beta_j$  denotes the transcript specific correction the characteristic translation rate, and  $K_X$   
605 denotes a translation saturation constant. The characteristic maximum translation rate  
606 was defined as the product of a characteristic translation rate constant ( $k_X$ ) and the abun-  
607 dance of Ribosomes ( $RIBO$ ),  $V_X^{\max} = k_X (RIBO)$ , where both  $k_X$  and  $RIBO$  abundance  
608 were estimated from literature (Milo *et al.*, 2010).

609 The signaling and gene expression model equations were implemented in Julia and

610 solved using the CVODE routine of the Sundials package (Bezanson *et al.*, 2014, Hindmarsh  
611 *et al.*, 2005). The model code and parameter ensemble is freely available under an MIT  
612 software license and can be downloaded from <http://www.varnerlab.org>.

613 *Estimation of model parameters using multiobjective optimization.* The EMT model had  
614 296 unknown parameters (169 kinetic constants, 44 saturation constants, 38 control logic  
615 paramters, and 45 non-zero initial conditions) which were not uniquely identifiable given  
616 the training data. Instead, we estimated a population of likely models (each consistent  
617 with the training data) using 41 data sets generated in DLD1 colon carcinoma, MDCKII,  
618 and A375 melanoma cells taken from Medici *et al.* (Medici *et al.*, 2008). We used the  
619 Pareto Optimal Ensemble Technique (JuPOETs) multiobjective optimization framework in  
620 combination with leave-one-out cross-validation to estimate an ensemble of model param-  
621 eters (Song *et al.*, 2010). Cross-validation was used to calculate both training and predic-  
622 tion error during the parameter estimation procedure (Kohavi, 1995). The 41 intracellular  
623 protein and mRNA data-sets used for identification were organized into 11 objective func-  
624 tions. These 11 objective functions were then partitioned, where each partition contained  
625 ten training objectives and one validation objective. The training and validation data were  
626 Western blots. We achived a physical simulation scale by establishing characteristic rates  
627 of transcription, translation, mRNA and protein degradation, as well as characteristic con-  
628 centrations of ribosomes and RNAPs (Milo *et al.*, 2010). The concentration scale is in nM,  
629 with proteins ranging from 10-1000nM and mRNA ranging from 0.01 to 1nM, reflecting the  
630 true abundances and ratios between each species.

631 **Cell culture and experimental interrogation** DLD1 colon carcinoma, MCF10A, and  
632 HUVEC were acquired from the American Tissue Culture Collection (Manassas, VA).  
633 Cells were grown in culture with RPMI 1640 medium with 10% fetal bovine serum and  
634 1% penicillin/streptomycin for DLD1, EBM-2 supplemented with EGM-2, 5% fetal bovine  
635 serum, and 1% penicillin/streptomycin for HUVEC, or MGEM 2 supplemented with insulin,  
636 bovine pituitary extract, cholera toxin, hEGF, hydrocortisone, 5% horse serum, and 1%

637 penicillin/streptomycin for MCF10A. Cells were serum starved for 24 hours and removed  
638 from all experimental conditions. Recombinant VEGFA165 was also removed from cul-  
639 ture medium prior to experimentation. Recombinant human TGF- $\beta$ 2 (R & D Systems,  
640 Minneapolis, MN) was added to the culture medium at a concentration of 10 ng/ml and re-  
641 combinant VEGFA165 at a concentration of (5ng/ml, 50ng/ml) for all relative experiments.  
642 NFAT inhibitor (VIVIT peptide) (EMDBiosciences, Darmstadt, Germany), was added to  
643 the culture medium at a concentration of 10 $\mu$ M for all relative experiments. Cells were  
644 passaged 1:3 or 1:4 every 3-6 d and used between passages 4 and 8.

645 *VEGF treatment* DLD1 and MCF10A cells were suspended in culture media (with RPMI  
646 1640 medium with 10% fetal bovine serum and 1% penicillin/streptomycin for DLD1 or  
647 MGEM 2 supplemented with insulin, bovine pituitary extract, cholera toxin, hEGF, hydro-  
648 cortisone, 5% horse serum, and 1% penicillin/streptomycin for MCF10A), and allowed to  
649 aggregate overnight in hanging drop culture (20 $\mu$ L; 20,000 cells). The spherical aggre-  
650 gates were placed on the surface of neutralized type I collagen hydrogels (1.5mg/mL)  
651 and allowed to adhere. Cultures were then serum starved (1% serum) for 24 hours. Re-  
652 combinant VEGFA165 was then added to the media (5ng/ml, 50ng/ml) and mRNA was  
653 harvested after 3hr and 24hr timepoint.

654 *RT-PCR* RNA extractions were performed using a Qiagen total RNA purification kit (Qi-  
655 agen, Valencia, CA) and RNA was reverse transcribed to cDNA using the SuperScript  
656 III RT-PCR kit with oligo(dT) primer (Invitrogen). Sufficient quality RNA was determined  
657 by an absorbance ratio A260/A280 of 1.8-2.1, while the quantity of RNA was determined  
658 by measuring the absorbance at 260nm (A260). Real-time PCR experiments were con-  
659 ducted using the SYBR Green PCR system (Biorad, Hercules, CA) on a Biorad CFX96  
660 cycler, with 40 cycles per sample. Cycling temperatures were as follows: denaturing,  
661 95C; annealing, 60C; and extension, 70C. Primers were designed to detect GAPDH, E-  
662 cadherin, vimentin, Slug, Sp1, and NFATc1 in cDNA clones: Sp1 (F-TTG AAA AAG GAG  
663 TTG GTG GC, R-TGC TGG TTC TGT AAG TTG GG, Accession NG030361.1), NFATc1

664 (F-GCA TCA CAG GGA AGA CCG TGT C, R-GAA GTT CAA TGT CGG AGT TTC TGA  
665 G, Accession NG029226.1). GAPDH, E-cadherin, vimentin, and Slug primers were taken  
666 from previously published literature (Medici *et al.*, 2008).

667 *Antibody Staining* Samples were fixed in 4% PFA overnight at 4C. Samples were then  
668 washed for 15 minutes on a rocker 3 times with PBS, permeabilized with 0.2% Triton-X  
669 100 (VWR International, Radnor, PA) for 10 minutes, and washed another 3 times with  
670 PBS. Samples were incubated overnight at 4C in a 1% BSA (Rockland Immunochemi-  
671 cals, Inc., Gilbertsville, PA) blocking solution followed by another 4C overnight incubation  
672 with either rabbit anti-human E-cadherin 1:100 (Abcam, ab53033), mouse anti-human  
673 phospho-Sp1 1:100 (Abcam, ab37707), mouse anti-human vimentin 1:100 (Invitrogen,  
674 V9), and rabbit anti-human NFATc1 (Santa Cruz, sc-7294) 1:100. After 3 washes for 15  
675 minutes with PBS, samples were exposed to Alexa Fluor 488 or 568 conjugated (Invit-  
676 rogen), species specific secondary antibodies at 1:100 in 1% BSA for 2 hours at room  
677 temperature. Three more washes with PBS for 15 minutes were followed by incubation  
678 with either DRAQ5 far red nuclear stain (Enzo Life Sciences, Plymouth Meeting, PA) at  
679 1:1000.

680 *FACS* Flow cytometry for E-cadherin 1:100 (Abcam) and vimentin 1:100 expressing cells  
681 was performed. Briefly, cells were trypsinized, fixed with 4% PFA for 10 min and then pre-  
682 served in 50% methanol/PBS. Cells were kept in the -20C until antibody staining was  
683 preformed. Samples were divided into multiple aliquots in order to stain the proteins  
684 separately and compensate for secondary antibody non-specific binding. Cells were in-  
685 cubated for 24 hrs at 4 C in primary antibody diluted in either PBS (extracellular) or 0.2%  
686 saponin-PBS (intracellular). Cells were then washed 3 times with PBS and incubated  
687 with appropriate secondary antibodies and imaged using a Coulter Epics XL-MCL Flow  
688 Cytometer (Coulter). All samples were compensated using appropriate background sub-  
689 traction and all samples were normalized using 7500 cells per flow condition.

690 *Three-Dimensional Culture and Tubulogenesis Assays* For invasion/migration assays,  
691 cells were resuspended in culture media, and allowed to aggregate overnight in hanging  
692 drop culture ( $20\mu\text{L}$ ; 20,000 cells). The spherical aggregates were placed on the surface of  
693 neutralized type I collagen hydrogels (1.5mg/mL) and allowed to adhere for 2 hrs before  
694 adding treatments. Cultures were maintained for 72 hrs, after which they were fixed in  
695 4% PFA and slowly rehydrated using PBS. For compaction assays, cells were pelleted  
696 via centrifugation and resuspended within a neutralized collagen hydrogel (1.5mg/mL)  
697 solution at a density of 400,000 cells/mL.  $250\mu\text{L}$  of gel was inoculated into culture wells,  
698 which solidified after 60min. Treatments were then added within  $800\mu\text{L}$  of the culture  
699 medium without serum. Gels were liberated from the surfaces of the culture wells the  
700 next day and cultured free floating for an additional 3-7 days, exchanging serum free  
701 media with appropriate factors every 48 hrs.

702 Tubulogenesis was defined as a typical nonmalignant acini structure. This includes a  
703 polarized epithelial cell, hollow lumen, and the basal sides of the cell are surrounded by  
704 ECM proteins (Fig. 6A, Controls or VEGF treated). Previous work has shown that change  
705 in the morphological characteristics of nontumorigenic MCF10A epithelial acini occur over  
706 time and exploiting them to growth in 3D culture can be quantified. For example, using  
707 image segmentation, Chang et al. (Chang *et al.*, 2007) examined the elongation of the  
708 MCF10A acini at 6, 12, and 96 hours after a particular treatment. Polizzotti et al. (Poliz-  
709 zotti *et al.*, 2012) also suggested a computational method to quantify acini structure based  
710 on morphological characteristics in nonmalignant, noninvasive, and invasive conditions.  
711 Adapted from these approaches, we first fluorescently labeled our cultures and captured  
712 the acini structures by 3D confocal microscopy. Next individual acini structures in the im-  
713 ages were segmented by imageJ and labeled. We then extracted the number of ductal  
714 branches. Ductal branching was defined as any elongated cell cluster extending away  
715 from the total acini structure, which was manually segmented and counted using ImageJ.  
716 A total of 5 images for each condition were used, and approximately 12 acini were ana-

<sup>717</sup> lyzed in each image. Total branching was normalized to the amount of acini present, and  
<sup>718</sup> provides an overall general assessment to the extent of acini remodeling.

<sup>719</sup> **Statistics** Results are expressed as mean  $\pm$  standard error,  $n \geq 6$ . Data was analyzed  
<sup>720</sup> with the GraphPad Prism version 4.00 for Windows (GraphPad Software, San Diego,  
<sup>721</sup> CA) and SAS (Statistical Analysis Software, Cary, NC). A one-way ANOVA with Tukey's  
<sup>722</sup> post hoc was used to compare differences between means and data was transformed  
<sup>723</sup> when necessary to obtain equal sample variances. Differences between means were  
<sup>724</sup> considered significant at  $p < 0.05$ .

725 **References**

- 726 Abramoff M, Magelhaes P, Ram S (2004) Image Processing with ImageJ. *Biophotonics International*, **11**: 36–42
- 727 Ahmed S, Nawshad A (2007) Complexity in interpretation of embryonic epithelial-mesenchymal transition in response to transforming growth factor-beta signaling. *Cells Tissues Organs* **185**: 131–45
- 728 729 730 Aramburu J, Yaffe MB, López-Rodríguez C, Cantley LC, Hogan PG, Rao A (1999) Affinity-driven peptide selection of an NFAT inhibitor more selective than cyclosporin A. *Science* **285**: 2129–33
- 731 732 733 Arce L, Pate KT, Waterman ML (2009) Groucho binds two conserved regions of LEF-1 for HDAC-dependent repression. *BMC Cancer* **9**: 159
- 734 Bailey JE (2001) Complex biology with no parameters. *Nat Biotechnol* **19**: 503–4
- 735 Bassen D, Vilkovoy M, Minot M, Butcher JT, Varner JD (2016) JuPOETs: A Constrained Multiobjective Optimization Approach to Estimate Biochemical Model Ensembles in the Julia Programming Language. *bioRxiv* **10.1101/056044**
- 736 Bezanson J, Edelman A, Karpinski S, Shah VB (2014) Julia: A Fresh Approach to Numerical Computing. *CoRR* **abs/1411.1607**
- 737 Bullock MD, Sayan AE, Packham GK, Mirnezami AH (2012) MicroRNAs: critical regulators of epithelial to mesenchymal (EMT) and mesenchymal to epithelial transition (MET) in cancer progression. *Biol Cell* **104**: 3–12
- 738 739 740 741 742 743 744 745 746 747 748 749 750 751 Butcher JT, Penrod AM, García AJ, Nerem RM (2004) Unique morphology and focal adhesion development of valvular endothelial cells in static and fluid flow environments. *Arterioscler Thromb Vasc Biol* **24**: 1429–34
- Cano A, Pérez-Moreno MA, Rodrigo I, Locascio A, Blanco MJ, del Barrio MG, Portillo F, Nieto MA (2000) The transcription factor snail controls epithelial-mesenchymal transitions by repressing E-cadherin expression. *Nat Cell Biol* **2**: 76–83
- Chang H, Park C, Parvin B (2007) Quantitative Representation of Three-dimensional Cell

- 752 Culture Models. In *Proceedings of the 2007 IEEE International Symposium on Biomed-*  
753 *ical Imaging: From Nano to Macro, Washington, DC, USA, April 12-16, 2007*. pp. 89–92
- 754 Chen WW, Schoeberl B, Jasper PJ, Niepel M, Nielsen UB, Lauffenburger DA, Sorger PK  
755 (2009) Input-output behavior of ErbB signaling pathways as revealed by a mass action  
756 model trained against dynamic data. *Mol Syst Biol* **5**: 239
- 757 Choi M, Shi J, Jung SH, Chen X, Cho KH (2012) Attractor landscape analysis reveals  
758 feedback loops in the p53 network that control the cellular response to DNA damage.  
759 *Sci Signal* **5**: ra83
- 760 Chung SW, Miles FL, Sikes RA, Cooper CR, Farach-Carson MC, Ogunnaike BA (2009)  
761 Quantitative modeling and analysis of the transforming growth factor beta signaling  
762 pathway. *Biophys J* **96**: 1733–50
- 763 Cirit M, Haugh JM (2012) Data-driven modelling of receptor tyrosine kinase signalling  
764 networks quantifies receptor-specific potencies of PI3K- and Ras-dependent ERK acti-  
765 vation. *Biochem J* **441**: 77–85
- 766 Creixell P, Schoof EM, Erler JT, Linding R (2012) Navigating cancer network attractors for  
767 tumor-specific therapy. *Nat Biotechnol* **30**: 842–8
- 768 Debnath J, Brugge JS (2005) Modelling glandular epithelial cancers in three-dimensional  
769 cultures. *Nat Rev Cancer* **5**: 675–88
- 770 Debnath J, Muthuswamy SK, Brugge JS (2003) Morphogenesis and oncogenesis of MCF-  
771 10A mammary epithelial acini grown in three-dimensional basement membrane cul-  
772 tures. *Methods* **30**: 256–268
- 773 Derynck R, Zhang YE (2003) Smad-dependent and Smad-independent pathways in TGF-  
774 beta family signalling. *Nature* **425**: 577–84
- 775 Dhasarathy A, Phadke D, Mav D, Shah RR, Wade PA (2011) The transcription factors  
776 Snail and Slug activate the transforming growth factor-beta signaling pathway in breast  
777 cancer. *PLoS One* **6**: e26514
- 778 Dhimolea E, Maffini MV, Soto AM, Sonnenschein C (2010) The role of collagen reorgani-

- 779 zation on mammary epithelial morphogenesis in a 3D culture model. *Biomaterials* **31**:  
780 3622–3630
- 781 Eastman Q, Grosschedl R (1999) Regulation of LEF-1/TCF transcription factors by Wnt  
782 and other signals. *Curr Opin Cell Biol* **11**: 233–40
- 783 Eisenberg LM, Markwald RR (1995) Molecular regulation of atrioventricular valvuloseptal  
784 morphogenesis. *Circ Res* **77**: 1–6
- 785 Ferrara N (2002) VEGF and the quest for tumour angiogenesis factors. *Nat Rev Cancer*  
786 **2**: 795–803
- 787 Gadkar KG, Varner J, Doyle FJ 3rd (2005) Model identification of signal transduction  
788 networks from data using a state regulator problem. *Syst Biol (Stevenage)* **2**: 17–30
- 789 Grumolato L, Liu G, Haremaiki T, Mungamuri SK, Mong P, Akiri G, Lopez-Bergami P, Arita  
790 A, Anouar Y, Mlodzik M, Ronai ZA, Brody J, Weinstein DC, Aaronson SA (2013) ?-  
791 Catenin-Independent Activation of TCF1/LEF1 in Human Hematopoietic Tumor Cells  
792 through Interaction with ATF2 Transcription Factors. *PLoS Genet* **9**: e1003603
- 793 Guaita S, Puig I, Franci C, Garrido M, Dominguez D, Batlle E, Sancho E, Dedhar S,  
794 De Herreros AG, Baulida J (2002) Snail induction of epithelial to mesenchymal transition  
795 in tumor cells is accompanied by MUC1 repression and ZEB1 expression. *J Biol Chem*  
796 **277**: 39209–16
- 797 Handl J, Kell DB, Knowles J (2007) Multiobjective optimization in bioinformatics and com-  
798 putational biology. *IEEE/ACM Trans Comput Biol Bioinform* **4**: 279–92
- 799 Hardy KM, Booth BW, Hendrix MJC, Salomon DS, Strizzi L (2010) ErbB/EGF signaling  
800 and EMT in mammary development and breast cancer. *J Mammary Gland Biol Neo-*  
801 *plasia* **15**: 191–9
- 802 Hasenauer J, Waldherr S, Doszczak M, Radde N, Scheurich P, Allgöwer F (2011) Iden-  
803 tification of models of heterogeneous cell populations from population snapshot data.  
804 *BMC Bioinformatics* **12**: 125
- 805 Hemavathy K, Ashraf SI, Ip YT (2000a) Snail/slug family of repressors: slowly going into

- 806 the fast lane of development and cancer. *Gene* **257**: 1–12
- 807 Hemavathy K, Guru SC, Harris J, Chen JD, Ip YT (2000b) Human Slug is a repressor that  
808 localizes to sites of active transcription. *Mol Cell Biol* **20**: 5087–95
- 809 Hindmarsh A, Brown P, Grant K, Lee S, Serban R, Shumaker D, Woodward C (2005) SUN-  
810 DIALS: Suite of nonlinear and differential/algebraic equation solvers. *ACM Transactions  
811 on Mathematical Software* **31**: 363–396
- 812 Hong JP, Li XM, Li MX, Zheng FL (2013) VEGF suppresses epithelial-mesenchymal tran-  
813 sition by inhibiting the expression of Smad3 and miR-192 a Smad3-dependent mi-  
814 croRNA. *Int J Mol Med* **31**: 1436–42
- 815 Huber MA, Azoitei N, Baumann B, Grünert S, Sommer A, Pehamberger H, Kraut N, Beug  
816 H, Wirth T (2004) NF-kappaB is essential for epithelial-mesenchymal transition and  
817 metastasis in a model of breast cancer progression. *J Clin Invest* **114**: 569–81
- 818 Hyduke DR, Palsson BØ (2010) Towards genome-scale signalling network reconstruc-  
819 tions. *Nat Rev Genet* **11**: 297–307
- 820 Jackstadt R, Röh S, Neumann J, Jung P, Hoffmann R, Horst D, Berens C, Bornkamm  
821 GW, Kirchner T, Menssen A, Hermeking H (2013) AP4 is a mediator of epithelial-  
822 mesenchymal transition and metastasis in colorectal cancer. *J Exp Med* **210**: 1331–50
- 823 Jensen LJ, Kuhn M, Stark M, Chaffron S, Creevey C, Muller J, Doerks T, Julien P, Roth  
824 A, Simonovic M, Bork P, von Mering C (2009) STRING 8—a global view on proteins and  
825 their functional interactions in 630 organisms. *Nucleic Acids Res* **37**: D412–6
- 826 Jiang YG, Luo Y, He DI, Li X, Zhang LI, Peng T, Li MC, Lin YH (2007) Role of Wnt/beta-  
827 catenin signaling pathway in epithelial-mesenchymal transition of human prostate can-  
828 cer induced by hypoxia-inducible factor-1alpha. *Int J Urol* **14**: 1034–9
- 829 Kalita MK, Sargsyan K, Tian B, Paulucci-Holthauzen A, Najm HN, Debusschere BJ,  
830 Brasier AR (2011) Sources of cell-to-cell variability in canonical nuclear factor-kB (NF-  
831 kB) signaling pathway inferred from single cell dynamic images. *J Biol Chem* **286**:  
832 37741–57

- 833 Kim K, Lu Z, Hay ED (2002) Direct evidence for a role of beta-catenin/LEF-1 signaling  
834 pathway in induction of EMT. *Cell Biol Int* **26**: 463–76
- 835 Kohavi R (1995) A study of cross-validation and bootstrap for accuracy estimation and  
836 model selection. In *International joint Conference on artificial intelligence*, vol. 14. Cite-  
837 seer, pp. 1137–1145
- 838 Larue L, Bellacosa A (2005) Epithelial-mesenchymal transition in development and can-  
839 cer: role of phosphatidylinositol 3' kinase/AKT pathways. *Oncogene* **24**: 7443–54
- 840 Lee MW, Vassiliadis VS, Park JM (2009) Individual-based and stochastic modeling of cell  
841 population dynamics considering substrate dependency. *Biotechnol Bioeng* **103**: 891–9
- 842 Lequieu J, Chakrabarti A, Nayak S, Varner JD (2011) Computational modeling and anal-  
843 ysis of insulin induced eukaryotic translation initiation. *PLoS Comput Biol* **7**: e1002263
- 844 Lian Yg, Zhou Qg, Zhang Yj, Zheng Fl (2011) VEGF ameliorates tubulointerstitial fibrosis  
845 in unilateral ureteral obstruction mice via inhibition of epithelial-mesenchymal transition.  
846 *Acta Pharmacol Sin* **32**: 1513–21
- 847 Linding R, Jensen LJ, Osthimer GJ, van Vugt MATM, Jørgensen C, Miron IM, Diella F,  
848 Colwill K, Taylor L, Elder K, Metalnikov P, Nguyen V, Pascalescu A, Jin J, Park JG, Sam-  
849 son LD, Woodgett JR, Russell RB, Bork P, Yaffe MB, et al. (2007) Systematic discovery  
850 of in vivo phosphorylation networks. *Cell* **129**: 1415–26
- 851 Luan D, Szlam F, Tanaka KA, Barie PS, Varner JD (2010) Ensembles of uncertain mathe-  
852 matical models can identify network response to therapeutic interventions. *Mol Biosyst*  
853 **6**: 2272–86
- 854 Machta BB, Chachra R, Transtrum MK, Sethna JP (2013) Parameter space compression  
855 underlies emergent theories and predictive models. *Science* **342**: 604–7
- 856 Mancini M, Toker A (2009) NFAT proteins: emerging roles in cancer progression. *Nat Rev*  
857 *Cancer* **9**: 810–820
- 858 Massagué J, Seoane J, Wotton D (2005) Smad transcription factors. *Genes Dev* **19**:  
859 2783–810

- 860 Medici D, Hay ED, Goodenough DA (2006) Cooperation between snail and LEF-1 trans-  
861cription factors is essential for TGF-beta1-induced epithelial-mesenchymal transition.  
862 *Mol Biol Cell* **17**: 1871–9
- 863 Medici D, Hay ED, Olsen BR (2008) Snail and Slug promote epithelial-mesenchymal tran-  
864sition through beta-catenin-T-cell factor-4-dependent expression of transforming growth  
865 factor-beta3. *Mol Biol Cell* **19**: 4875–87
- 866 Medici D, Potenta S, Kalluri R (2011) Transforming growth factor-?2 promotes  
867 Snail-mediated endothelial-mesenchymal transition through convergence of Smad-  
868 dependent and Smad-independent signalling. *Biochem J* **437**: 515–520
- 869 Milo R, Jorgensen P, Moran U, Weber G, Springer M (2010) BioNumbers—the database  
870 of key numbers in molecular and cell biology. *Nucleic Acids Res* **38**: D750–3
- 871 Moles CG, Mendes P, Banga JR (2003) Parameter estimation in biochemical pathways: a  
872 comparison of global optimization methods. *Genome Res* **13**: 2467–74
- 873 Morris MK, Saez-Rodriguez J, Clarke DC, Sorger PK, Lauffenburger DA (2011) Training  
874 signaling pathway maps to biochemical data with constrained fuzzy logic: quantitative  
875 analysis of liver cell responses to inflammatory stimuli. *PLoS Comput Biol* **7**: e1001099
- 876 Nagy JA, Dvorak AM, Dvorak HF (2007) VEGF-A and the induction of pathological angio-  
877 genesis. *Annu Rev Pathol* **2**: 251–75
- 878 Nawshad A, Hay ED (2003) TGFbeta3 signaling activates transcription of the LEF1 gene  
879 to induce epithelial mesenchymal transformation during mouse palate development. *J  
880 Cell Biol* **163**: 1291–301
- 881 Nawshad A, Medici D, Liu CC, Hay ED (2007) TGFbeta3 inhibits E-cadherin gene expres-  
882 sion in palate medial-edge epithelial cells through a Smad2-Smad4-LEF1 transcription  
883 complex. *J Cell Sci* **120**: 1646–53
- 884 Neve RM, Chin K, Fridlyand J, Yeh J, Baehner FL, Fevr T, Clark L, Bayani N, Coppe JP,  
885 Tong F, Speed T, Spellman PT, DeVries S, Lapuk A, Wang NJ, Kuo WL, Stilwell JL,  
886 Pinkel D, Albertson DG, Waldman FM, *et al.* (2006) A collection of breast cancer cell

- 887 lines for the study of functionally distinct cancer subtypes. *Cancer Cell* **10**: 515–27
- 888 Niessen K, Fu Y, Chang L, Hoodless PA, McFadden D, Karsan A (2008) Slug is a direct  
889 Notch target required for initiation of cardiac cushion cellularization. *J Cell Biol* **182**:  
890 315–25
- 891 O'Brien LE, Tang K, Kats ES, Schutz-Geschwender A, Lipschutz JH, Mostov KE (2004)  
892 ERK and MMPs sequentially regulate distinct stages of epithelial tubule development.  
893 *Dev Cell* **7**: 21–32
- 894 Park SY, Lee HE, Li H, Shipitsin M, Gelman R, Polyak K (2010) Heterogeneity for stem  
895 cell-related markers according to tumor subtype and histologic stage in breast cancer.  
896 *Clin Cancer Res* **16**: 876–87
- 897 Pearson GW, Hunter T (2007) Real-time imaging reveals that noninvasive mammary ep-  
898 ithelial acini can contain motile cells. *J Cell Biol* **179**: 1555–67
- 899 Polizzotti L, Basak O, Bjornsson C, Shubert K, Yener B, Plopper G (2012) Novel Image  
900 Analysis Approach Quantifies Morphological Characteristics of 3D Breast Culture Acini  
901 with Varying Metastatic Potentials. *J Biomed Biotech* **2012**: 1–16
- 902 Polyak K, Weinberg RA (2009) Transitions between epithelial and mesenchymal states:  
903 acquisition of malignant and stem cell traits. *Nat Rev Cancer* **9**: 265–273
- 904 Rodriguez-Fernandez M, Rehberg M, Kremling A, Banga JR (2013) Simultaneous model  
905 discrimination and parameter estimation in dynamic models of cellular systems. *BMC  
906 Syst Biol* **7**: 76
- 907 Sagar A, Varner JD (2015) Dynamic Modeling of the Human Coagulation Cascade Using  
908 Reduced Order Effective Kinetic Models. *Processes* **3**: 178
- 909 Sainani KL (2012) Meet the Skeptics: Why some doubt biomedical models - and what it  
910 takes to win them over. *Biomedical Computation Review* : 12 – 18
- 911 Schoeberl B, Eichler-Jonsson C, Gilles ED, Muller G (2002) Computational modeling of  
912 the dynamics of the MAP kinase cascade activated by surface and internalized EGF  
913 receptors. *Nat Biotechnol* **20**: 370–375

- 914 Singh G, Singh SK, König A, Reutlinger K, Nye MD, Adhikary T, Eilers M, Gress TM,  
915 Fernandez-Zapico ME, Ellenrieder V (2010) Sequential activation of NFAT and c-Myc  
916 transcription factors mediates the TGF-beta switch from a suppressor to a promoter of  
917 cancer cell proliferation. *J Biol Chem* **285**: 27241–50
- 918 Song SO, Chakrabarti A, Varner JD (2010) Ensembles of signal transduction models  
919 using Pareto Optimal Ensemble Techniques (POETs). *Biotechnol J* **5**: 768–80
- 920 Stahl PJ, Felsen D (2001) Transforming growth factor-beta, basement membrane, and  
921 epithelial-mesenchymal transdifferentiation: implications for fibrosis in kidney disease.  
922 *Am J Pathol* **159**: 1187–92
- 923 Strauss R, Li ZY, Liu Y, Beyer I, Persson J, Sova P, Möller T, Pesonen S, Hemminki A,  
924 Hamerlik P, Drescher C, Urban N, Bartek J, Lieber A (2011) Analysis of epithelial and  
925 mesenchymal markers in ovarian cancer reveals phenotypic heterogeneity and plastic-  
926 ity. *PLoS One* **6**: e16186
- 927 Suehiro Ji, Kanki Y, Makihara C, Schadler K, Miura M, Manabe Y, Aburatani H, Kodama  
928 T, Minami T (2014) Genome-wide approaches reveal functional vascular endothelial  
929 growth factor (VEGF)-inducible nuclear factor of activated T cells (NFAT) c1 binding to  
930 angiogenesis-related genes in the endothelium. *J Biol Chem* **289**: 29044–59
- 931 Sullivan NJ, Sasser AK, Axel AE, Vesuna F, Raman V, Ramirez N, Oberyszyn TM, Hall BM  
932 (2009) Interleukin-6 induces an epithelial-mesenchymal transition phenotype in human  
933 breast cancer cells. *Oncogene* **28**: 2940–7
- 934 Swain PS, Elowitz MB, Siggia ED (2002) Intrinsic and extrinsic contributions to stochas-  
935 ticity in gene expression. *Proc Natl Acad Sci U S A* **99**: 12795–800
- 936 Tasseff R, Nayak S, Song SO, Yen A, Varner JD (2011) Modeling and analysis of retinoic  
937 acid induced differentiation of uncommitted precursor cells. *Integr Biol (Camb)* **3**: 578–  
938 591
- 939 Terfve C, Cokelaer T, Henriques D, MacNamara A, Goncalves E, Morris MK, van Iersel M,  
940 Lauffenburger DA, Saez-Rodriguez J (2012) CellNOptR: a flexible toolkit to train protein

- 941 signaling networks to data using multiple logic formalisms. *BMC Syst Biol* **6**: 133
- 942 Thiery JP (2003) Epithelial-mesenchymal transitions in development and pathologies.
- 943 *Curr Opin Cell Biol* **15**: 740–6
- 944 Vega S, Morales AV, Ocaña OH, Valdés F, Fabregat I, Nieto MA (2004) Snail blocks the
- 945 cell cycle and confers resistance to cell death. *Genes Dev* **18**: 1131–43
- 946 Vilar JMG, Jansen R, Sander C (2006) Signal processing in the TGF-beta superfamily
- 947 ligand-receptor network. *PLoS Comput Biol* **2**: e3
- 948 Villaverde AF, Banga JR (2014) Reverse engineering and identification in systems biology:
- 949 strategies, perspectives and challenges. *J R Soc Interface* **11**: 20130505
- 950 Wayman J, Varner J (2013) Biological systems modeling of metabolic and signaling net-
- 951 works. *Curr Opin Chem Eng* **2**: 365 – 372
- 952 Welch-Reardon KM, Wu N, Hughes CCW (2014) A Role for Partial Endothelial-
- 953 Mesenchymal Transitions in Angiogenesis? *Arterioscler Thromb Vasc Biol*
- 954 Willis BC, Borok Z (2007) TGF-beta-induced EMT: mechanisms and implications for fi-
- 955 brotic lung disease. *Am J Physiol Lung Cell Mol Physiol* **293**: L525–34
- 956 Wu Y, Deng J, Rychahou PG, Qiu S, Evers BM, Zhou BP (2009) Stabilization of snail by
- 957 NF-kappaB is required for inflammation-induced cell migration and invasion. *Cancer*
- 958 *Cell* **15**: 416–28
- 959 Xu J, Lamouille S, Derynck R (2009) TGF-beta-induced epithelial to mesenchymal transi-
- 960 tion. *Cell Res* **19**: 156–72
- 961 Zajchowski DA, Bartholdi MF, Gong Y, Webster L, Liu HL, Munishkin A, Beauheim C,
- 962 Harvey S, Ethier SP, Johnson PH (2001) Identification of gene expression profiles that
- 963 predict the aggressive behavior of breast cancer cells. *Cancer Res* **61**: 5168–78
- 964 Zavadil J, Böttlinger EP (2005) TGF-beta and epithelial-to-mesenchymal transitions.
- 965 *Oncogene* **24**: 5764–74
- 966 Zhou BP, Deng J, Xia W, Xu J, Li YM, Gunduz M, Hung MC (2004) Dual regulation of Snail
- 967 by GSK-3beta-mediated phosphorylation in control of epithelial-mesenchymal transi-

968 tion. *Nat Cell Biol* **6**: 931–40

## Extracellular

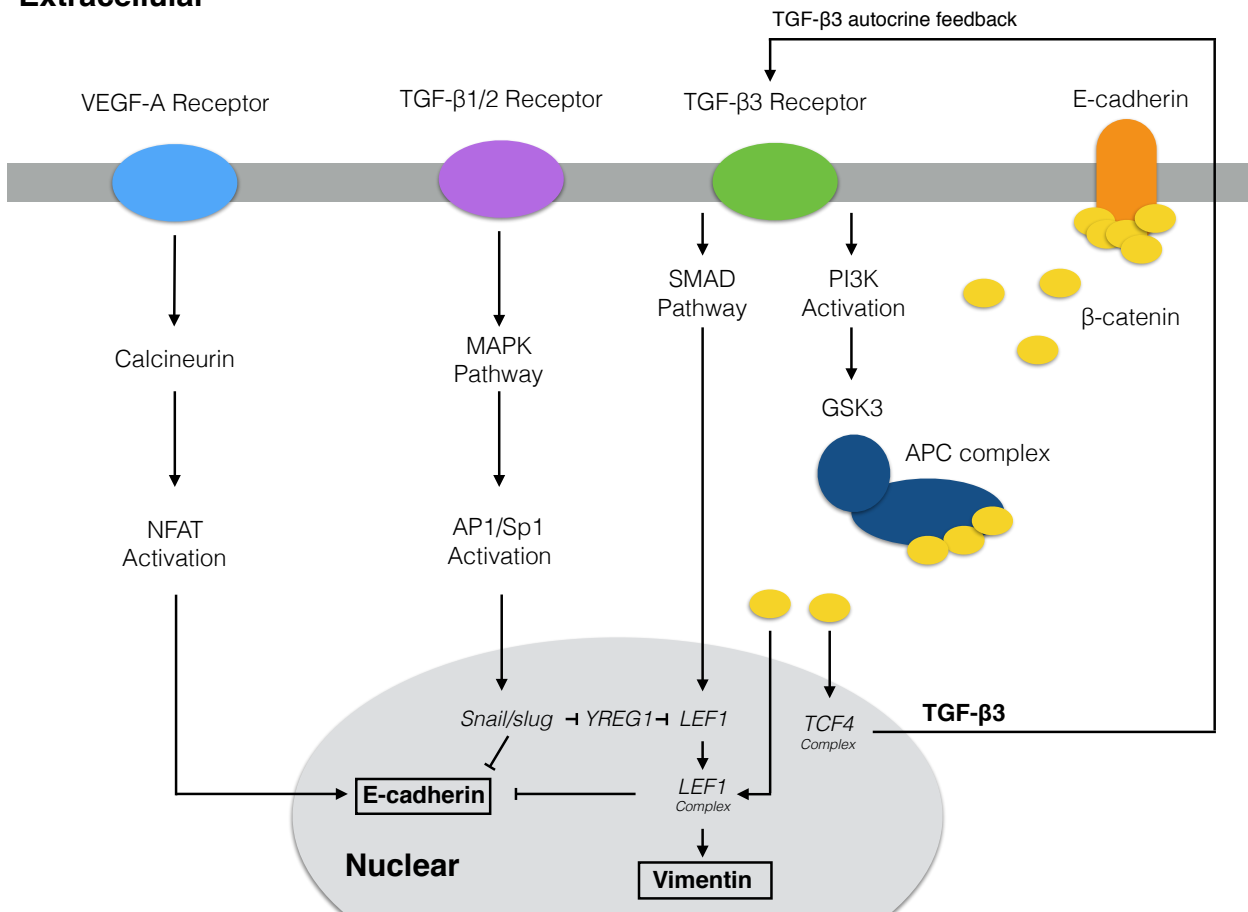


**Fig. 1:** Model connectivity recreates the core architecture during EMT. The EMT network contains 97 nodes (proteins, mRNA, and genes) interconnected by 169 interactions. Central to EMT induction, activation of the MAPK cascade occurs through TGF- $\beta$ 1/2 binding which activates the AP-1/Sp1 transcriptional axis. AP-1/Sp1 drives an autocrine response of TGF- $\beta$ 3, which activates the Smad cascade, leading to phenotypic change. Conversely, VEGF-A binding can stabilize an epithelial phenotype through NFAT activation. Downstream activation of  $\beta$ -catenin signaling due to E-cadherin loss and GSK3 inactivation of  $\beta$ -cateinin confinement is critical to the complete activation of the EMT program. The complete list of molecular interactions that comprise the model is given in the supplement.

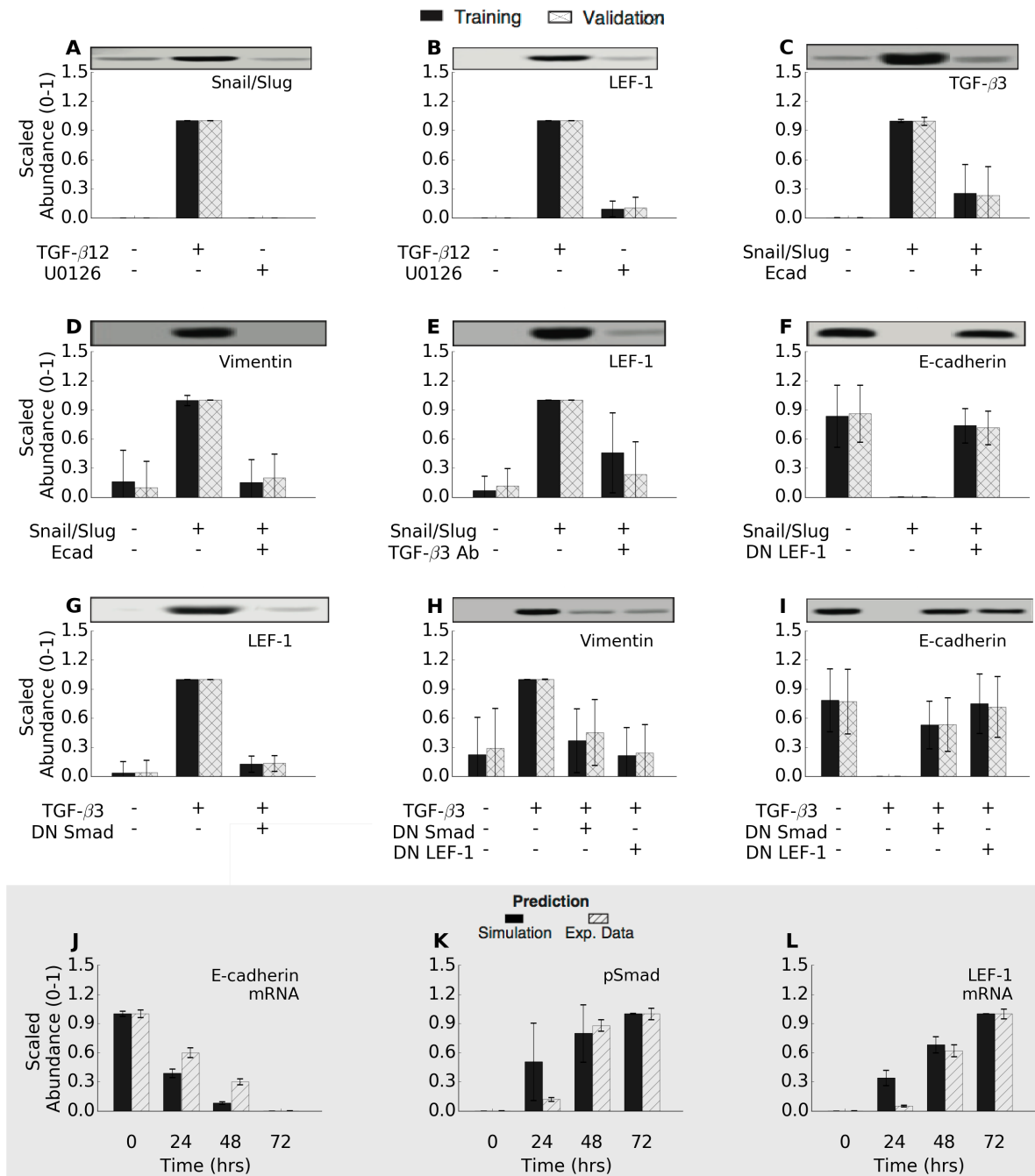


**Fig. 2:** Training and validation simulations. The population of EMT models qualitatively captured TGF- $\beta$ -induced EMT signaling. (A-I) The population was generated using JuPOETs and trained using 11 different objective functions (41 data sets) taken from Medici *et al.* (Medici *et al.*, 2008). The model captured the simulated experiments for 72% of the cases. (J-L) The model populations were also compared against untrained temporal data to measure the effectiveness as a pure prediction.

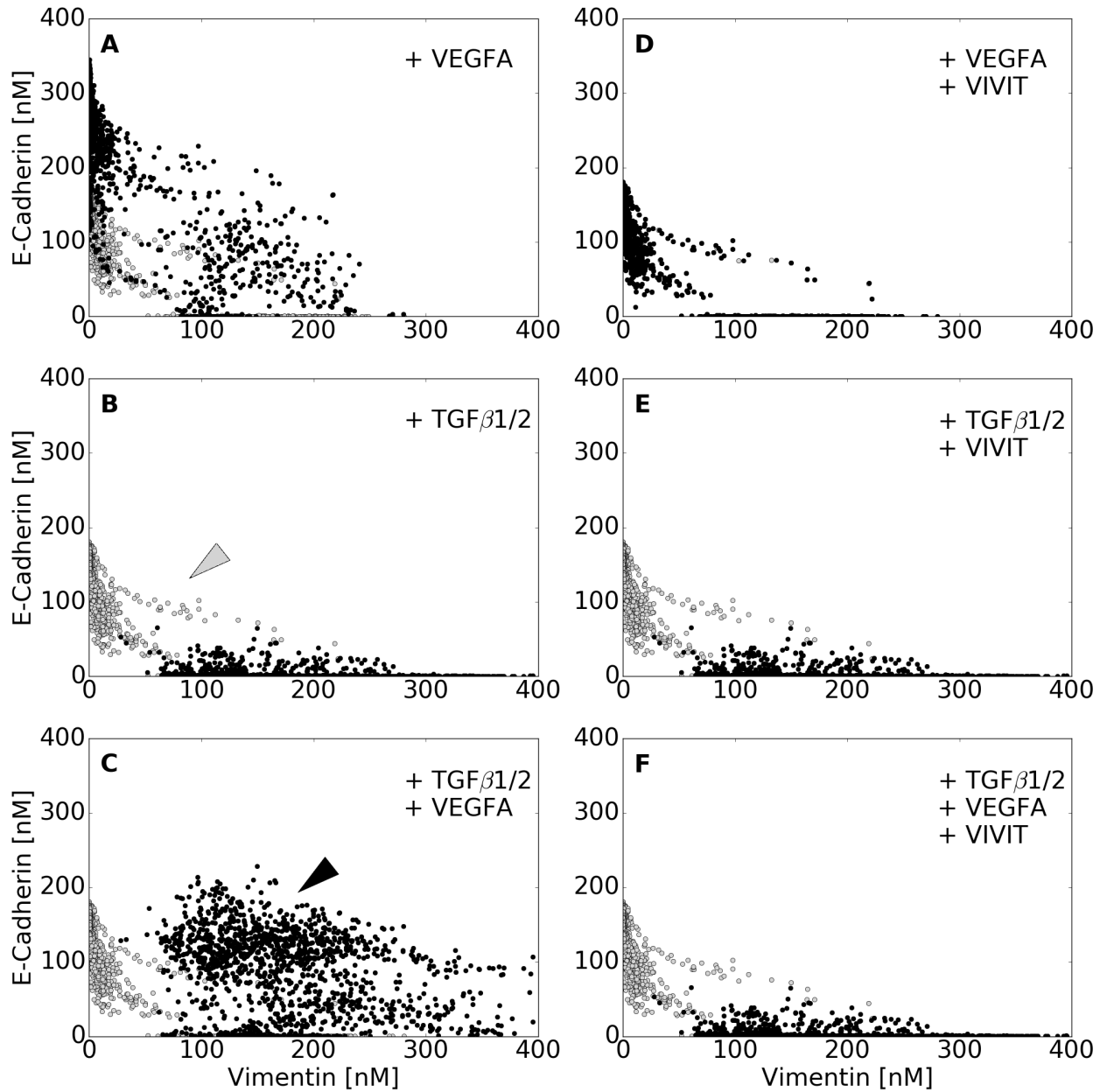


**Fig. 3:** Simulated VEGF-A and TGF- $\beta$ 1/2 exposure promoted phenotype heterogeneity. Simulated response to TGF- $\beta$ 1/2 and VEGF-A exposure with and without axis specific inhibitors. Vimentin and E-cadherin abundances (in nM) were used to quantify the shift in population at 48 hrs. (A-C) VEGF-A (50 a.u.) treatment resulted in a population with enhanced epithelial properties. This was contrary to the addition of TGF- $\beta$ 2 (10 a.u.), which shifted the population towards a mesenchymal phenotype. Interestingly, the combined effects of TGF- $\beta$ 2 and VEGFA was found to increase both ecadherin and vimentin levels, creating a heterogeneous population (black arrow), which can also be seen in a minority of untreated cells (gray arrow). (D-F) To isolate the effect of NFAT, we inhibited NFAT de-phosphorylation in combination with VEGFA. This negated the increase in ecadherin expression and shifted the population towards a mesenchymal phenotype (Q1,Q3). Likewise, combining NFAT inhibition with TGF- $\beta$  mitigated all VEGF enhanced ecadherin expression. Lastly, combination of TGF- $\beta$ 2, VEGFA, and NFAT inhibition nearly mitigated all effects of VEGFA, shifting the heterogeneous population towards a mesenchymal phenotype. In whole, high levels of phosphorylated-Sp1 correlated with vimentin expression, while NFAT was responsible for maintaining E-cadherin expression, although neither were mutually exclusive.

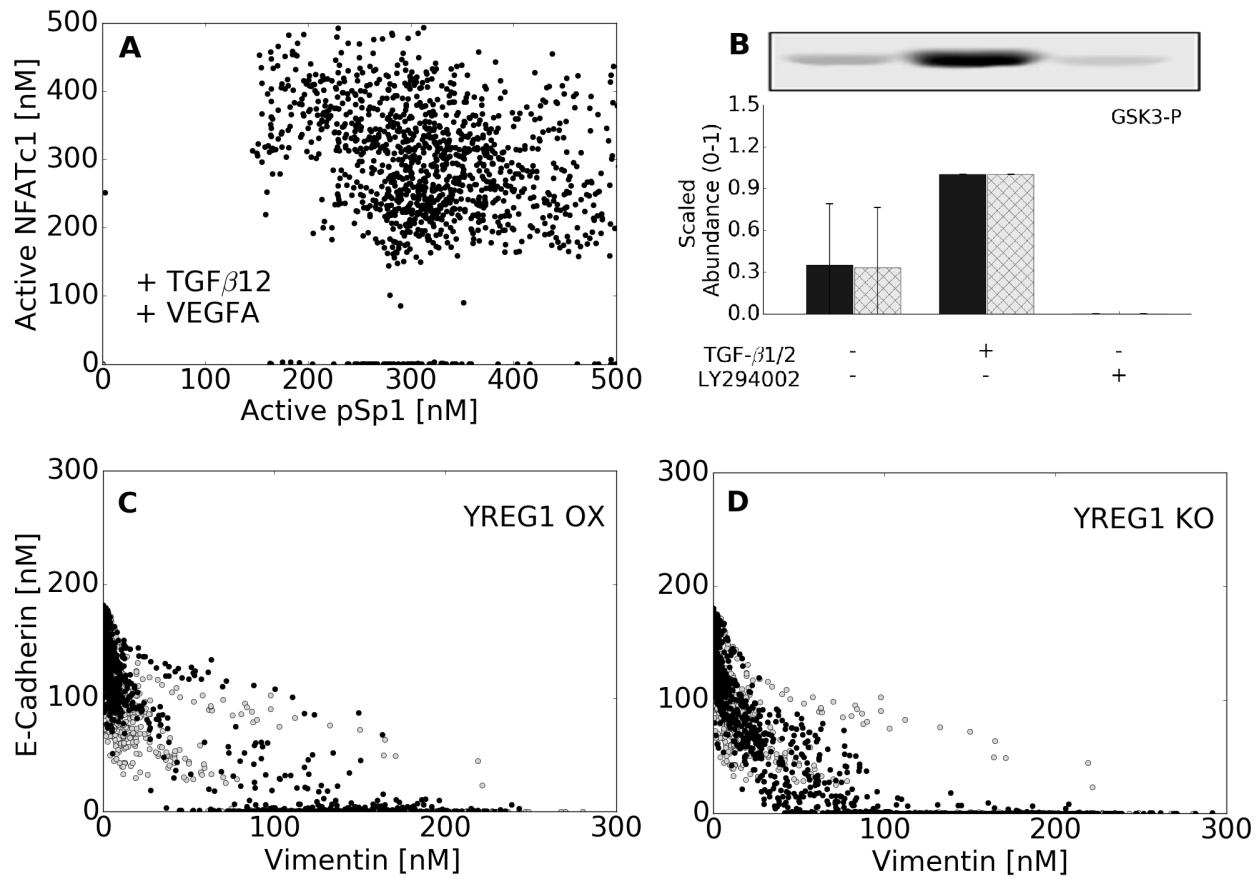


**Fig. 4:** Analysis of underlying signaling responses. (A) We examined the distribution of NFATc1 and AP1/SP1 in cells containing the hybrid phenotype (VEGF-A + TGF- $\beta$ 2 case), showing the potential for cells to express both SP1 and NFATc1 in a non exclusive manner. (B) We were able to show a fit to an additional objective demonstrating the activation of GSK3 through PI3K. Our model captures this activation through TGF- $\beta$ 3 signaling. LY294002 is a PI3K inhibitor. (C) We identified a novel regulator of LEF1 called YREG1 that allows Snail/Slug to emulate an inducer by repressing YREG1, which was required to stabilize the untreated population. YREG1 overexpression revealed an enhanced epithelial phenotype, while some inherently transformed cells moved towards a hybrid phenotype. (D) In the absence of YREG1, most of the population failed to consistently retain a stable epithelial state.

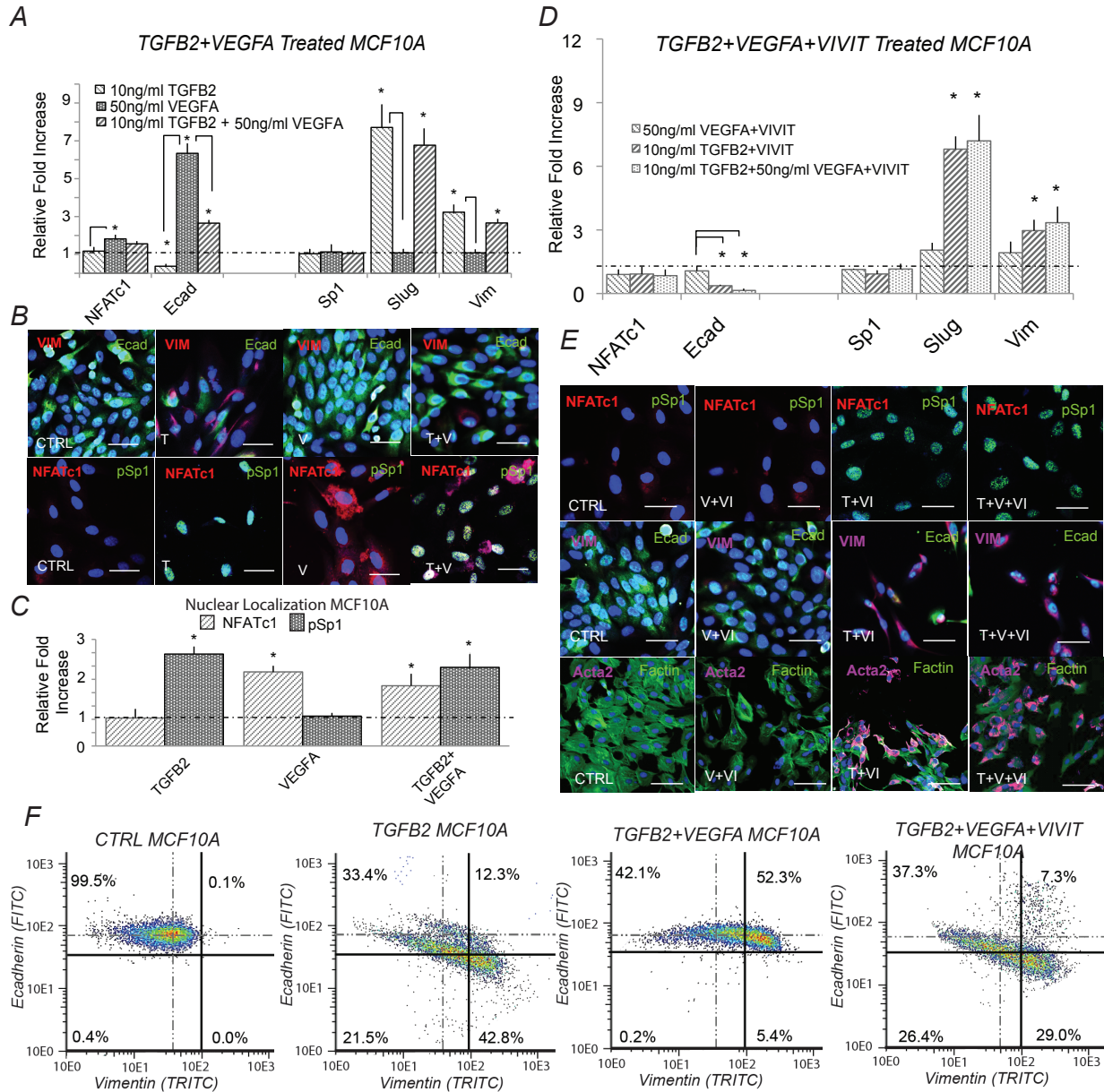


**Fig. 5:** Simultaneous TGF- $\beta$ 1/2 and VEGF-A treatment induced phenotype heterogeneity and is dependent upon NFAT activity *in-vitro*. (A) In MCF10A, treatment with (10ng/ml) TGF- $\beta$ 2 increased Slug and vimentin, while ecadherin expression was inhibited at both the gene and protein level at 48 hrs. Conversely, VEGFA alone increased both NFATc1 and ecadherin gene expression. Simultaneous TGF- $\beta$ 2 (10ng/ml) and VEGFA (50ng/ml) treatment increased Slug, NFATc1, and vimentin expression, while also increasing ecadherin levels via qPCR. (B-C) Immunofluorescence confirmed these results and nuclear co-localization of both phospho-Sp1 and NFAT were found dependent upon TGF- $\beta$ 2 and VEGFA, respectively. (D) To isolate the effect of NFAT, treatment of VEGFA (50ng/ml) and VIVIT (10 $\mu$ M) reduced ecadherin expression at 48hrs (control-dashed line). Similarly, combined TGF- $\beta$ 2, VEGFA and VIVIT treatment increased Slug and vimentin expression, while inhibiting ecadherin levels via qPCR. (E) These findings were confirmed via immunofluorescence as the VIVIT peptide inhibited ecadherin and nuclear localization of NFATc1 in all three cases. (F) Quantitative flow cytometry also confirmed this trend. Similar experiments in DLD1 followed a similar trend (supplement). Magnification, 40x. Scale bars: 50 $\mu$ m. C=Control, T=TGF- $\beta$ 2 , V=VEGFA, VI= NFAT inhibitor (VIVIT). Asterisks signify statistical differences from each other according to a one-way ANOVA with Tukey's post hoc ( $p < 0.05$ ).

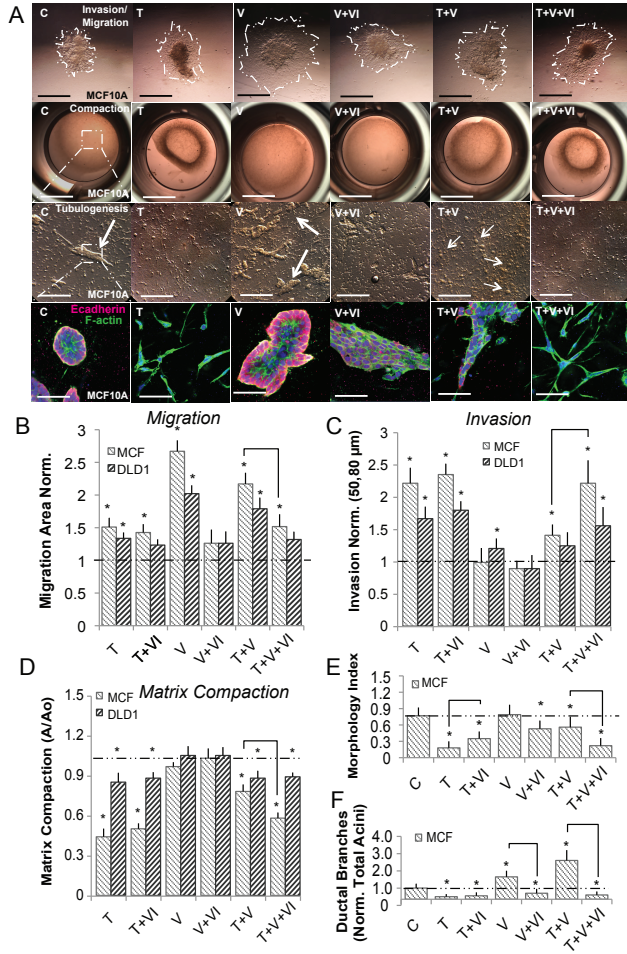


**Fig. 6:** Ductal branching is dependent upon phenotype heterogeneity within MCF10A in 3-D culture. MCF10A and DLD1 were formed into spheroids overnight and explanted to a collagen gel for 72 hrs. For compaction and tubular assays, cells were embedded into collagen gels for 72 hrs, and the extent of tubulogenesis was measured at 7 days. (A-D) Within MCF10A, TGF- $\beta$ 2 (10ng/ml) enhanced invasion and contractile properties while, VEGFA (50ng/ml) promoted increased migration. TGF- $\beta$ 2 with VEGFA significantly increased migration, while limiting with compaction. VIVIT (10 $\mu$ M) in combination with VEGFA and TGF- $\beta$ 2 decreased migration and compaction, while increasing invasion. (D) Likewise, cell morphology (circularity index) correlated with both invasion and compaction in MCF10A. (E-F) The size of tubular structures (acini) also increased significantly upon addition of VEGFA, while the number of ductal branches was most significant upon simultaneous TGF- $\beta$ 2 and VEGFA treatment (Red-Ecadherin, Green-Factin, Blue-Nuclear). DLD1 cells followed a similar trend, although the degree of migration, invasion, and compaction was less significant. In addition, no tubular structures were identified during the 7 day tubulogenesis endpoints. Scale bars: 500 $\mu$ m, 1000 $\mu$ m, 250 $\mu$ m, and 80 $\mu$ m, respectively. C=Control, T=TGF- $\beta$ 2 , V=VEGFA, VI= NFAT inhibitor (VIVIT). Asterisks signify statistical differences from each other according to a one-way ANOVA with Tukey's post hoc ( $p < 0.05$ ). Boxes in the left-most panel identify regions identified by arrows that were then imaged in greater zoom in the panel immediately below. The box diagram was not repeated for arrows in the other panels for clarity, but the same method was applied.

969 **Supplemental Materials and Methods**

970 **Estimation and cross-validation of EMT model parameters.** We used the Pareto Opt-  
971 imal Ensemble Technique (POETs) multiobjective optimization framework in combina-  
972 tion with leave-one-out cross-validation to estimate an ensemble of TGF- $\beta$ /EMT models.  
973 Cross-validation was used to calculate both training and prediction error during the pa-  
974 rameter estimation procedure (Kohavi, 1995). The 41 intracellular protein and mRNA  
975 data-sets used for identification were organized into 11 objective functions. These 11  
976 objective functions were then partitioned, where each partition contained ten training ob-  
977 jectives and one validation objective. POETs integrates standard search strategies e.g.,  
978 Simulated Annealing (SA) or Pattern Search (PS) with a Pareto-rank fitness assignment  
979 (Bassen *et al.*, 2016, Song *et al.*, 2010). Denote a candidate parameter set at iteration  
980  $i + 1$  as  $\mathbf{k}_{i+1}$ . The squared error for  $\mathbf{k}_{i+1}$  for training set  $j$  was defined as:

$$E_j(\mathbf{k}) = \sum_{i=1}^{\mathcal{T}_j} \left( \hat{\mathcal{M}}_{ij} - \hat{y}_{ij}(\mathbf{k}) \right)^2 \quad (\text{S1})$$

981 The symbol  $\hat{\mathcal{M}}_{ij}$  denotes scaled experimental observations (from training set  $j$ ) while  
982  $\hat{y}_{ij}$  denotes the scaled simulation output (from training set  $j$ ). The quantity  $i$  denotes  
983 the sampled time-index and  $\mathcal{T}_j$  denotes the number of time points for experiment  $j$ . In  
984 this study, the experimental data used for model training was typically the band intensity  
985 from Western or Northern blots. Band intensity was estimated using the ImageJ software  
986 package Abramoff *et al.* (2004). The scaled measurement for species  $x$  at time  $i =$   
987  $\{t_1, t_2, \dots, t_n\}$  in condition  $j$  is given by:

$$\hat{\mathcal{M}}_{ij} = \frac{\mathcal{M}_{ij} - \min_i \mathcal{M}_{ij}}{\max_i \mathcal{M}_{ij} - \min_i \mathcal{M}_{ij}} \quad (\text{S2})$$

988 Under this scaling, the lowest intensity band equaled zero while the highest intensity  
989 band equaled one. A similar scaling was defined for the simulation output. By doing this  
990 scaling, we trained the model on the relative change in blot intensity, over conditions or

O#	Species (protein)	Cell Type	Training	Prediction	Random
O1	LEF1	DLD1 CC,MDCKII,A375 MC	0.54 ± 0.167	0.505 ± 0.175	1.765 ± 0.223
O2	Vimentin	DLD1 CC,MDCKII,A375 MC	1.044 ± 0.668	0.783 ± 0.666	2.098 ± 0.784
O3	TGF $\beta$ 3	DLD1 CC,MDCKII,A375 MC	0.119 ± 0.262	0.225 ± 0.418	1.408 ± 0.732
O4	E-cadherin	DLD1 CC,MDCKII,A375 MC	2.299 ± 0.449	2.154 ± 0.625	3.459 ± 0.643
O5	$\beta$ -catenin	DLD1 CC,MDCKII,A375 MC	0.752 ± 0.38	0.514 ± 0.351	1.025 ± 0.0
O6	TGF $\beta$ 3	DLD1 CC,MDCKII,A375 MC	1.662 ± 0.55	1.54 ± 0.677	3.328 ± 0.981
O7	GSK3-P	DLD1 CC,MDCKII,A375 MC	0.19 ± 0.291	0.203 ± 0.292	0.756 ± 0.309
O8	LEF1	DLD1 CC,MDCKII,A375 MC	0.023 ± 0.078	0.03 ± 0.11	0.937 ± 0.298
O9	E-Cadherin	DLD1 CC,MDCKII,A375 MC	1.092 ± 1.228	1.412 ± 1.348	2.652 ± 1.435
O10	Snail/Slug	DLD1 CC,MDCKII,A375 MC	0.019 ± 0.0	0.019 ± 0.0	1.111 ± 0.744
O11	LEF1	DLD1 CC,MDCKII,A375 MC	0.005 ± 0.015	0.013 ± 0.06	0.797 ± 0.431

**Fig. S1:** Training and prediction values as a function of condition for the 11 TGF- $\beta$  objective functions versus a random parameter control.

991 time (depending upon the experiment). Thus, when using multiple data sets (possibly from  
 992 different sources) that were qualitatively similar but quantitatively different e.g., slightly  
 993 different blot intensities over time or condition, we captured the underlying trends in the  
 994 scaled data.

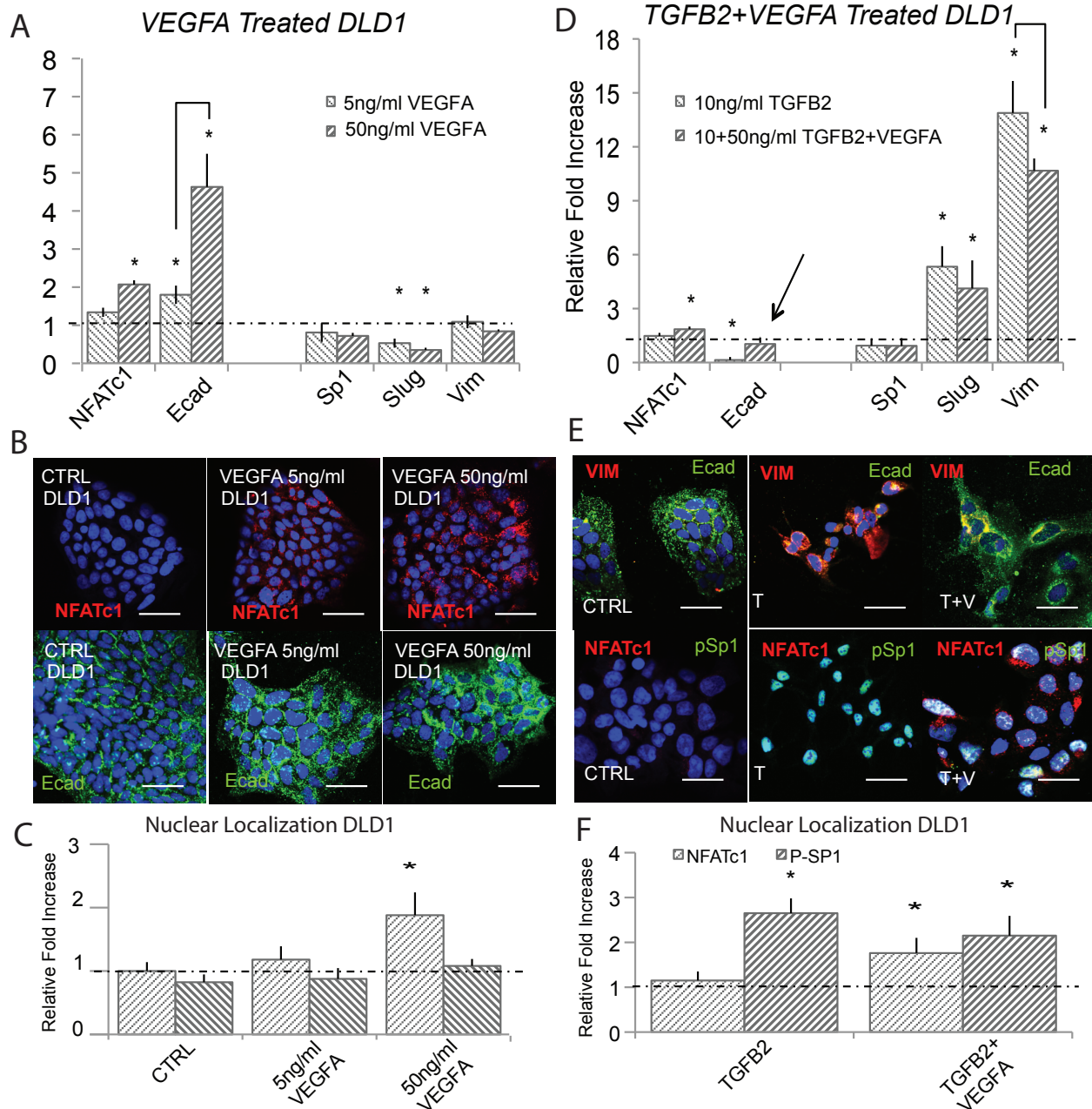


**Fig. S2:** VEGF-A attenuates TGF- $\beta$ 1/2 to induce phenotype heterogeneity in DLD1. (A) In DLD1, we found that 5ng/ml of VEGFA increased NFATc1 and E-cadherin gene expression via qPCR and 50ng/ml potentiated this effect at 48 hrs. (B - C) These findings were confirmed at the protein level via immunofluorescence, as ecadherin levels and nuclear localization of NFATc1 increased. (D) Treatment with (10ng/ml) TGF $\beta$ 2 resulted in mesenchymal transformation as measured via qPCR against target genes Slug, ecadherin, vimentin, Sp1, and NFATc1. (E - F) Immunofluorescence and nuclear localization revealed a strong presence of phospho-Sp1. (G) Combination of VEGFA (50ng/ml) and TGF $\beta$ 2 (10ng/ml) treatment resulted in increased Slug, NFATc1, and vimentin expression, while also increasing ecadherin levels compared to control. (H) Immunofluorescence confirmed these results, as both ecadherin and vimentin levels were elevated. (I) A significant increase in nuclear localization of both NFATc1 and phospho-Sp1 were also found. Magnification, 40x. Scale bars: 50 $\mu$ m. C=Control, T=TGF $\beta$ 2 , V=VEGFA, VI=NFAT inhibitor (VIVIT). Asterisks signify statistical differences from each other according to a one-way ANOVA with Tukey's post hoc ( $p < 0.05$ ).

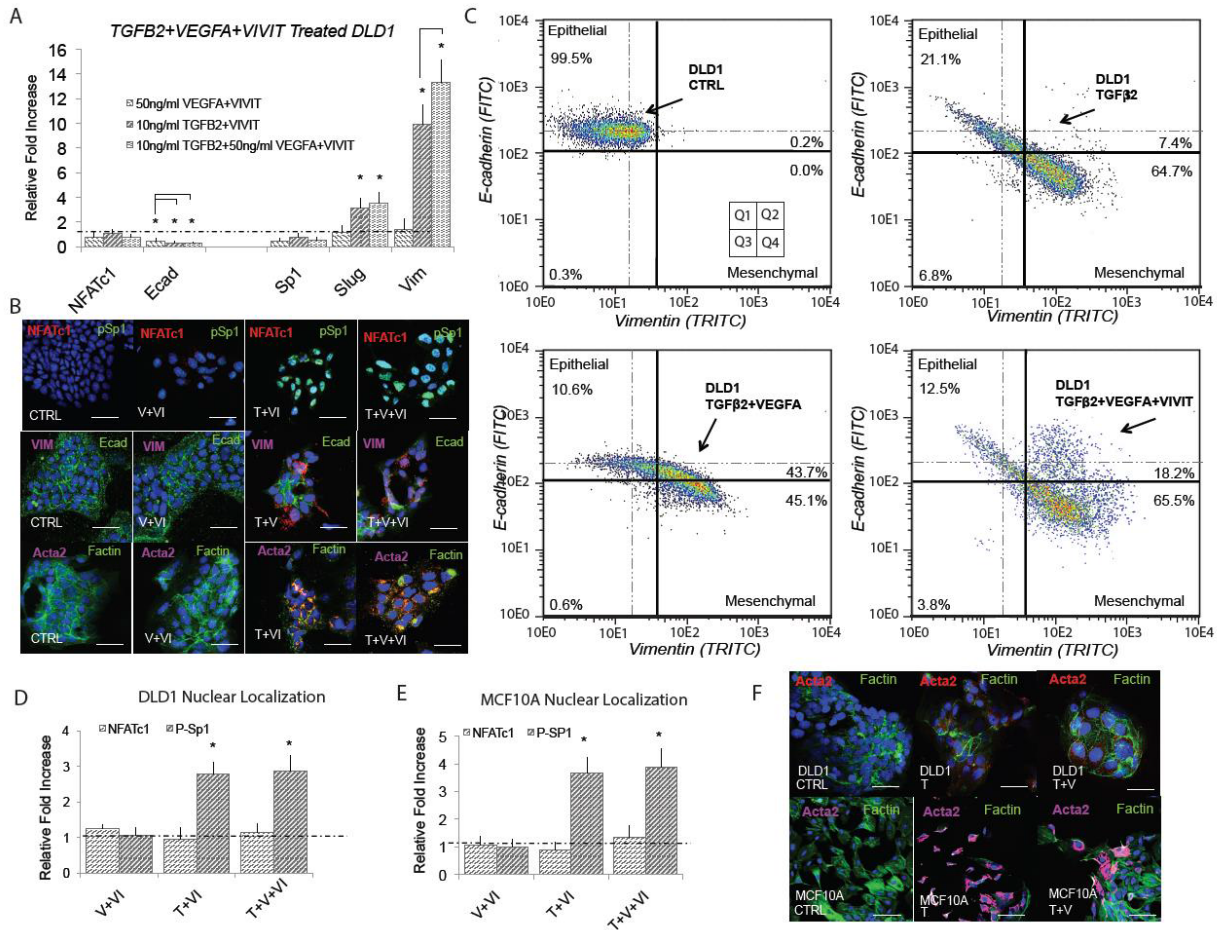


**Fig. S3:** E-cadherin expression is dependent upon NFAT activity in DLD1. (A) Treatment with VEGFA (50ng/ml) and NFAT inhibitory peptide VIVIT (10μM) resulted in significantly reduced ecadherin expression (qRT-PCR at 48hrs). Addition of TGF $\beta$ 2 (10ng/ml) and VIVIT resulted in increased Slug and vimentin expression, while inhibiting ecadherin levels. Combined TGF $\beta$ 2, VEGFA, and VIVIT treatment resulted in target genes Slug and vimentin expression increased, while inhibiting ecadherin levels. No change in Sp1 or NFATc1 expression was found. (B) These findings were confirmed via immunofluorescence as the VIVIT inhibitors was shown to inhibit ecadherin levels in all three cases. We also found no change in gene or nuclear localization of NFATc1 in all three cases, while phospho-Sp1 was found to increase in both TGF $\beta$  conditions. (C) Quantitative flow cytometry also confirmed this trend. (D,E) TGF $\beta$ 2, VEGFA and VIVIT treatment in DLD1 and MCF10A resulted in no change of Sp1 expression or NFATc1 expression. (F) Likewise, no change in nuclear localization of NFAT in all three cases, however phospho-Sp1 was found to increase in both TGF $\beta$  conditions. Magnification, 40x. Scale bars: 50μm. C=Control, T=TGF $\beta$ 2 , V=VEGFA, VI= NFAT inhibitor (VIVIT). Asterisks signify statistical differences from each other according to a one-way ANOVA with Tukey's post hoc ( $p < 0.05$ ).

PRELIMINARY DATA USED TO HANDFIT RESPONSE OF VEGFA WITHIN SYSTEM

		MCF10A						
VEGFA		Relative mRNA			Normalized			
		Ecad	Slug	Vim	Ecad	Slug	Vim	
	5ng/ml	3HR	1.31	1.04	0.93	0.00	1.00	1.00
		48 HR	3.60	1.03	0.91	0.45	0.94	0.88
50ng/ml		3HR	1.37	0.92	0.88	0.01	0.25	0.71
		48 HR	6.34	0.88	0.76	1.00	0.00	0.00
Standard Deviation								
VEGFA		Relative mRNA			Normalized			
		Ecad	Slug	Vim	Ecad	Slug	Vim	
		5ng/ml	0.89	0.03	0.02	0.00	0.03	0.02
50ng/ml		3HR	0.78	0.03	0.27	0.10	0.03	0.26
		48 HR	0.11	0.10	0.53	0.00	0.03	0.43
VEGFA		Relative mRNA			Normalized			
		Ecad	Slug	Vim	Ecad	Slug	Vim	
5ng/ml		3HR	1.21	0.76	1.03	0.00	1.00	0.76
		48 HR	1.80	0.53	1.09	0.17	0.44	1.00
Standard Deviation								
VEGFA		Relative mRNA			Normalized			
		Ecad	Slug	Vim	Ecad	Slug	Vim	
		5ng/ml	0.80	0.10	0.18	0.00	0.13	0.13
50ng/ml		3HR	0.24	0.12	0.17	0.02	0.10	0.16
		48 HR	0.89	0.19	0.45	0.06	0.11	0.33
VEGFA		Absolute mRNA			Normalized			
		Ecad	Slug	Vim	Ecad	Slug	Vim	
5ng/ml		3HR	0.94	88.12	10.23	0.00	1.00	1.00
		48 HR	2.10	55.64	5.45	0.40	0.41	0.40
50ng/ml		3HR	1.44	64.10	8.43	0.17	0.56	0.77
		48 HR	3.85	33.40	2.32	1.00	0.00	0.00
Standard Deviation								
VEGFA		Absolute mRNA			Normalized			
		Ecad	Slug	Vim	Ecad	Slug	Vim	
		5ng/ml	0.21	22.34	2.45	0.00	0.25	0.24
50ng/ml		3HR	0.45	15.55	1.12	0.09	0.11	0.08
		48 HR	0.38	17.87	2.23	0.05	0.16	0.20
VEGFA		3HR	1.30	9.46	0.45	0.34	0.00	0.00

**Fig. S4:** VEGF-A qPCR data used to hand fit VEGF enhancement of E-cadherin expression. mRNA was harvested after 3hr and 24hr timepoint.